CRITICAL SPEEDS OF TURBOMACHINERY COMPUTER PREDICTIONS VS. EXPERIMENTAL MEASUREMENTS

by

John M. Vance

Professor of Mechanical Engineering

Texas A&M University

Brian T. Murphy

Technical Staff Member

Rocketdyne Corporation

and

Harley A. Tripp

Staff Research Engineer

Shell Development Company

Houston, Texas

John M. Vance is a Professor of Mechanical Engineering at Texas A&M University. He received his B.S.M.E. (1960), M.S.M.E. (1964) and Ph.D. (1967) degrees from the University of Texas at Austin.

Dr. Vance came to Texas A&M from the University of Florida, where he developed a Rotordynamics and Vibrations Laboratory and conducted research on squeeze-film bearing dampers, helicopter propulsion systems, and other topics related to rotordynamics of turbomachinery.

Prior to joining the Mechanical Engineering faculty at Florida, he worked for five years as a Mechanical Engineer in industry, holding positions at Armco Steel, Texaco Research, and Tracor, Incorporated.

Dr. Vance is currently conducting research on rotordynamics, electromagnetic shaft currents, and torsional vibrations in the Turbomachinery Laboratories at Texas A&M University. He has published more than forty technical articles and reports on rotordynamic instability, squeeze-film bearing dampers, vibration isolaters, and related subjects. He is an active consultant to industry and government laboratories, and has held eleven summer appointments at Pratt & Whitney Aircraft, USASTL (Helicopter Propulsion Lab, Ft. Eustis), Southwest Research Institute, and Shell Development Company. He organized the annual short course for industry at Texas A&M on "Rotordynamics of Turbomachinery," co-organized the biennial "Workshop on Rotordynamics Instability Problems in High Performance Turbomachinery," and is a member of the Advisory Committee for the Turbomachinery Symposium.

Dr. Vance was named the Dresser Industries Associate Professor at Texas A&M in 1979-1980, and was Associate Head of the Department of Mechanical Engineering in 1980-1981. He is a member of ASME and ASEE, and is a registered professional engineer in the States of Texas and Florida.

Brian T. Murphy received his B.S. degree in Mechanical Engineering from the University of Florida in 1978. He received an M.S. in 1981 and a Ph.D. in Mechanical Engineering from Texas A&M University in May of 1984.

Dr. Murphy is a member of the Technical Staff in the Rotordynamics Group of the Rocketdyne Division of Rockwell International. His primary responsibilities are in the area of advanced technology development in support of the high-pressure turbopump analyses for the Space Shuttle Main Engine (SSME) Development Program. Other responsibilities include the rotordynamics analysis and testing of a variety of high-technology rotating machinery systems.

Harley A. Tripp is in the Mechanical Engineering Group at Shell Development Company where he is involved with both research and field problems relating to rotor/bearing dynamics, machinery stress analysis, and vibration. In this capacity he has worked on a wide range of machinery problems for the various divisions of Shell Oil Company. Mr. Tripp joined Shell in 1966 after receiving his B.S. and M.S. degrees in Mechanical Engineering from the University of Mississippi.

ABSTRACT

As a result of a continuing demand for increased performance, modern turbomachines are sometimes designed to operate near a critical speed. Machines for petrochemical and natural gas service have been purchased and delivered which were later discovered to be operating so close to a critical speed as to cause difficulty in maintaining the rotor balance required to ensure acceptable vibration levels.

A serious requirement for an accurate critical speed prediction capability is thus indicated. Field experience has shown that the accuracy of computer predicted critical speeds of contemporary turbomachines is sometimes open to question.

Reports on research to experimentally verify existing computer programs for *a priori* critical speed prediction are almost nonexistent in the engineering literature.

Comparisons of state-of-the-art computer predictions of critical speeds are described herein, with experimental measurements on shafts and rotors of varying complexity. The models investigated range from a precision uniform shaft in the laboratory to an eight-stage centrifugal compressor rotor.

Modifications made to existing computer programs to improve the accuracy of predicted critical speeds are also discussed. Special care must be taken to properly define the rotor-mass elastic model, which depends on the features of the computer program employed. The accuracy of critical speed predictions is shown to depend on: 1) the accuracy of the free-free rotor vibration models, which depends on the accuracy of the rotor mass-elastic model, once the computer algorithm is optimized, 2) the accuracy of the bearing stiffness and damping coefficients, which are speed dependent in the case of fluid-film bearings, and 3) the accuracy of the dynamic properties of the foundation, which can be represented by a frequency-dependent impedance and which must be determined by experimental measurements. In the special case of tilt-pad bearings, existing data on the stiffness properties was found to be unsatisfactory. Measurements were made and the new results are reported herein.

Measurements made on one of the laboratory models, a three-disk rotor on tilt-pad bearings, showed subsynchronous whirl, which is not explainable by contemporary instability theory unless the tilt-pad bearings have significant cross-coupling and less damping than the available literature predicts.

INTRODUCTION

As a result of a continuing demand for increased performance, many modern turbomachines for petrochemical and natural gas service are now being designed for operation at shaft speeds approaching the second critical speed. In fact, machines have been purchased and delivered which were later discovered to be operating so close to a critical speed as to cause difficulty in maintaining the rotor balance required to ensure acceptable vibration levels.

Since most machines purchased for petrochemical and natural gas service are custom-designed, or are versions of previous machines modified to meet the special requirements of a particular application, the problem described above cannot be solved by standardizing mass-produced components.

A serious requirement for an accurate critical speed prediction capability is thus indicated. The tolerable error depends on the desired margin. For example, if operating speeds are to be at least fifteen percent away from any critical speed, and the probable error in critical speed prediction is plus or minus five percent, then the specified margin must be increased to twenty percent.

Experimental verification of results from existing computer programs for critical speed prediction is almost nonexistent in the engineering literature. In most cases where predicted and measured critical speeds are compared in the literature, it is for a purpose other than verifying the analysis. In fact, the parameters input to the programs (i.e., the rotor-bearing physical parameters) are usually adjusted as required to obtain the best agreement with meaured results. An example is found in reference [1], in which the average reported discrepancy between the measured and computed (before adjustment) natural frequencies of turbogenerator rotors was reported to be 33.18 percent.

In cases where the relative effects of varying design parameters are being investigated, the adjustment of parameters to produce a baseline case is completely justified. For accurate prediction of critical speeds, *a priori*, it is useless.

Comparisons have been made between state-of-the-art computer predictions of critical speeds and experimental measurements on shafts and rotors of varying complexity. As part of the effort, refinements and application rules for the computer programs have been developed to optimize their accuracy. Experimental techniques were also developed to maximize the repeatability and precision of the measurements.

Critical speeds are shaft speeds which coincide with the natural frequencies of the rotor-bearing system. In most real machines, the natural frequencies are speed dependent, since gyroscopic moments, fluid-film bearing stiffness, and fluid seal stiffness are all speed dependent.

It was found early in this investigation that even the capability to accurately predict the nonrotating natural frequencies of a rotor, suspended free-free (no bearings), was questionable. Furthermore, it is known that the prediction of fluid-film bearing and seal stiffness and damping is a complex technology of itself. The first part of this investigation (Phase I) compared computer predictions with experimental measurements of the free-free natural frequencies of selected shafts and rotors. Subsequently, state-of-the-art computations were compared with measurements from rotating machines on fluid-film bearings (Phase II).

It should be understood that the free-free modes of rotor vibration do not directly correspond to the critical speeds of rotors in fluid film bearings. The first two rotor critical speeds in many machines correspond to rigid body modes which have a free-free natural frequency of zero (see Appendix). The first nonzero free-free natural frequency is a bending mode which can be compared with the first actual bending mode of the rotor-bearing system only if the bearing stiffnesses are extremely low.

The free-free natural frequencies and modes are, however, an excellent way of checking the accuracy of the rotor mass-elastic model without involving uncertainties in the bearing parameters. It should be noted that the mass-elastic model can be in considerable error, without introducing any significant error into the computed critical speeds of rigid-body modes. In fact, the first critical speed of a machine with a stiff rotor can be predicted very accurately simply by estimating the total rotor mass and the bearing stiffness correctly. Consequently, good agreement between the calculated and measured values of the first critical speed *on bearings* is not necessarily an indicator that the mass-elastic model is accurate, or that the critical speeds of the higher modes will be accurately predicted.

PHASE I: FREE-FREE SHAFTS AND ROTORS

Computer Program

The most widely used type of computer program for calculating the critical speeds of rotating machinery is based on the transfer matrix method. The method was developed concurrently and independently in the 1940s by Myklestad, for calculating natural frequencies of airplane wings, and by Prohl, for calculating critical speeds of steam turbines. In its modern form, it has been adapted for high speed digital computers, and has the advantage of requiring considerably less computer memory space than other methods. It is thus especially well suited for the modern desktop computer.

Most versions of this type of program do not include the effect of damping (which is often small) in order to simplify calculations and speed computer execution. For the work in Phase I, a program without damping is justified since the experimental measurement of the free-free modes involves almost no damping. Versions which do include damping are

usually based on the recent work of Lund [2], and have the capability to predict rotordynamic instabilities as well as damped critical speeds. They require computer algorithms involving complex numbers. Such a program was written for Phase II of this work. It is described later in this paper, but the rotor mass-elastic model is identical to that in the program without damping.

Several different transfer matrix programs for calculating both the undamped and damped critical speeds in turbomachinery were availale to the authors. One of the programs without damping was selected for modification. The selected program was originally coded in FORTRAN, but was adapted for HP-BASIC so that it could be used on a Hewlett-Packard (HP) 9845 computer.

Refinements and modifications were made to improve the accuracy (as determined by experimental measurements) and speed (execution time required) of the program. The changes and modifications to this program, called "CRITSPEED" in its final version, are described in the following.

Effect of Disk/Shaft Attachment Flexibility

One of the usual assusmptions inherent to critical speed analysis is that disks and wheels attached to the shaft remain rigid in all the calculated modes of interest. A further assumption usually made is that the attachment of the disks to the shaft is also rigid, so that the disks remain normal to the shaft in all modes. There is some evidence in the recent literature that these assumptions are not always valid [4].

Based on a feeling that one additional degree of freedom for each floppy disk was considered to be sufficient to simulate this effect, and the program was modified to calculate the effect of flexibility in the attachment of disks to the shaft. The effect considered is shown in Figure 1. The local slope θ of the shaft is different from the angular deflection θ' of the disk by the amount α, due to a finite moment stiffness of the attachment, K_T (inch/lb/radian).

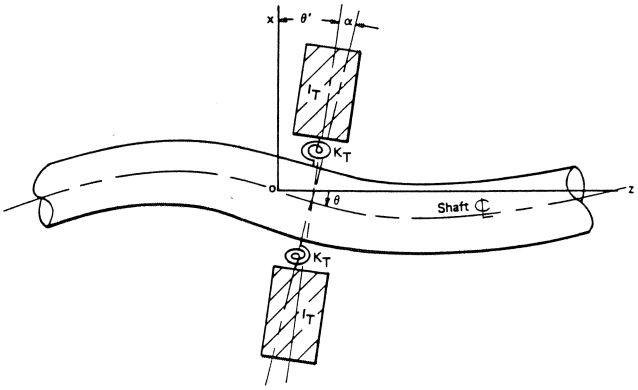

Figure 1. Disk Attachment of Flexibility Model.

The most straight forward analysis of the dynamic effect is to consider the mechanical mobility and impedance. By definition, the impedance of the rigid disk is:

$$Z_d = \frac{M}{\theta} = -I_T\omega^2 \tag{1}$$

where ω is the frequency of the local exciting moment, M.

For a rigid attachment, the moment transferred across the n^{th} disk in the computer program is

$$\begin{aligned} M_{n+1} &= M_n + Z_{dn}\theta_n \\ &= M_n - I_{Tn}\omega^2\theta_n \end{aligned} \tag{2}$$

For a flexible attachment, the moment stiffness K_T is in series with the inertia I_T. The resulting modified impedance of the disk is:

$$Z_d = \frac{1}{\bar{M}_K + \bar{M}_I} \tag{3}$$

where $\bar{M}_K = \dfrac{1}{K_T}$

and $\bar{M}_I = \dfrac{-1}{I_T\omega^2}$

are the mobilities of the attachment stiffness and disk inertia respectively. Thus,

$$Z_d = \frac{-K_T I_T \omega^2}{K_T - I_T\omega^2} \tag{4}$$

and the new transfer equation for the n^{th} disk is

$$\begin{aligned} M_{n+1} &= M_n + Z'_{d_n}\theta_n \\ &= M_n - \frac{K_T I_T \omega^2}{K_T - I_T\omega^2}\,\theta_n \end{aligned} \tag{5}$$

To utilize equation (5) in the program, a numerical value for the attachment stiffness, K_T, must be supplied. Three methods for calculating K_T have been used. Interestingly, all three of the cases investigated gave numbers of the same order of magnitude. The three methods are:

Calculation of the attachment stiffness based on an equation from the theory of elasticity [5]—This model is actually based on the bending of the disk itself.

The model, the equation, and associated values for the parameter α in the equation is shown in Figure 2, where

E = Young's modulus, psi
t = Disk thickness, in
μ = Poisson's ratio
r_s = Shaft radius, in
a = Radius of the disk, in
α = Shape factor

A quadratic curve has been derived to fit the data for the shape factor, α. The curve and its equation are shown in Figure 3, and are used in the program calculations.

Calculations based on an assumption that the disk attachment flexibility is a certain fraction of the local shaft moment flexibility—For the three-mass laboratory rotor (described later), accelerometer measurements on the disk indicated that the effective attachment stiffness was about twenty times the local shaft moment stiffness. Because the disks on this rotor are unusually thick, this number should be considered an upper limit.

For a concentrated moment midway between two simple supports, the local shaft moment stiffness is:

$$K_s = \frac{24EI}{\ell}$$

For any real case of practical interest, the effective length ℓ must be estimated. Then the attachment stiffness would be:

$$K_T \leqslant 20\ K_s \tag{6}$$

Selection of the value for K_T which produces calculated natural frequencies closest to the measured values—Although this method is not available to the typical user, it may be possible to establish values of K_T for various types of rotor construction, through experience. This method was used to verify methods 1 and 2.

Effect of Concentrated End Masses Due to the Definition of Rotor Stations in the Transfer Matrix Model

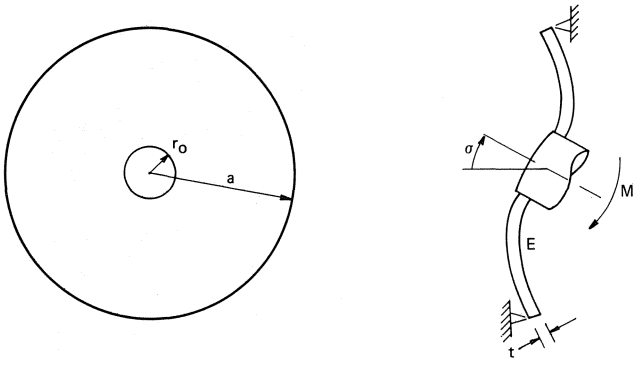

$$\sigma = \frac{M}{\alpha Et^3}, \quad \alpha = \alpha(r_o/a)$$

$$\text{So } K_T = \frac{M}{\sigma} = \alpha Et^3 \sim \frac{\text{in.-lb}}{\text{rad.}}$$

r_o/a	α (μ = 0.3, Steel)
0.1	0.713
0.15	0.945
0.20	1.22
0.25	1.56
0.30	2.00
0.35	2.56
0.40	3.32
0.50	5.93
0.55	8.23

Figure 2. Formula for K_T [5].

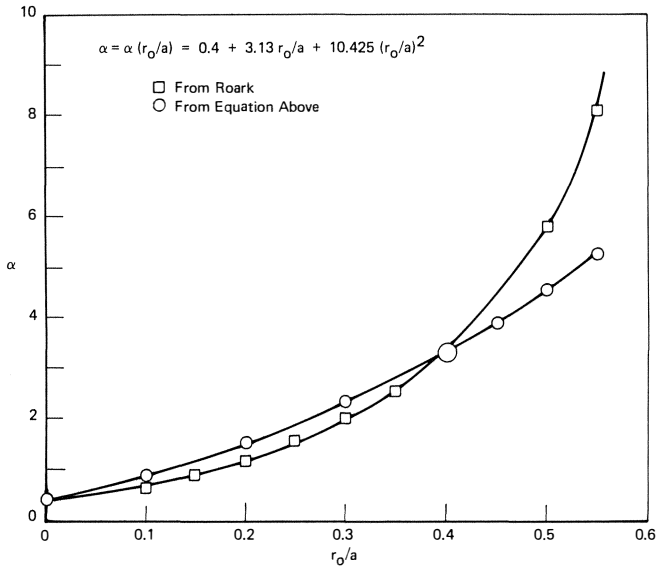

Figure 3. Shape Factor for $K_T = Et^3$.

The transfer matrix model for a uniform shaft of diameter D and length L, using only four stations (three segments) is shown in Figure 4. As usual, the last station on the right is of zero length.

A typical convention for lumping mass properties is to use one-half of the mass and mass moment of inertia from each of the shaft segments to the left and right of the station being considered. Using this convention gives:

$$m_1 = m_4 = \bar{\rho}L/6$$

$$m_2 = m_3 = \bar{\rho}L/3,$$

where $\bar{\rho}$ is the mass per unit length. Similarly,

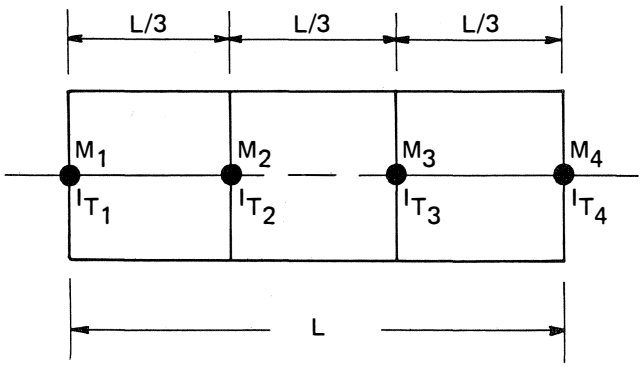

Figure 4. Transfer Matrix Model for a Uniform Shaft.

$$I_{T_1} = I_{T_4} = \frac{\bar{\rho}L}{6}\left(\frac{D^2}{16} + \frac{L^2}{108}\right)$$

and

$$I_{T_2} = I_{T_3} = \frac{\bar{\rho}L}{3}\left(\frac{D^2}{16} + \frac{L^2}{108}\right)$$

where the moments of inertia are taken about the centroids of the segments.

Using these values to calculate the total mass and resulting moment of inertia for the shaft gives

$$M = \sum_1^4 m_i = \bar{\rho}L \tag{7}$$

which is correct, and

$$I_T = \sum_1^4 I_{T_i} + 2m_2\left(\frac{L}{6}\right)^2 + 2m_1\left(\frac{L}{2}\right)^2 = \bar{\rho}L\left(\frac{D^2}{16} + \frac{L^2}{9}\right)$$

which is incorrect. The correct moment of inertia for the shaft is:

$$I_T = \bar{\rho}L\left(\frac{D^2}{16} + \frac{L^2}{12}\right) \tag{8}$$

The discrepancy is due to m_1 and m_4 being placed too far (further outboard) from the center of gravity (CG) of the shaft. This causes significant errors in the calculated natural frequencies when a small number of stations is used, especially for rigid rotor modes and for shafts with large masses near the ends. The evolution of a tendency by engineering analysts to use an inordinately large number of stations to model even simple rotors may be attributable to this effect.

A correction factor (f) has been derived to move part of the end mass to the next station inboard. Taking the left end station as an example, the corrected lumped masses m'_1 and m'_2 are

$$m'_1 = fm_1 \tag{9}$$

$$m'_2 = m_2 + (1-f)m_1 \tag{10}$$

$$f = \frac{1}{1 + \ell/4a} \tag{11}$$

where $\ell = \ell_1 + \ell_2$ (the length of segments 1 and 2),
a = distance from station 2 to the CG of the rotor.
If $\ell_1 \approx \ell_2$, and a $\approx$ L/2, where L is the total shaft length, then f is approximated by:

$$f = \frac{1}{1 + \ell_1/L} \tag{12}$$

Effect of Shear Deflection

For some rotating machinery, the geometry of the rotor is such that practically all of the shaft deflection is due to bend-

ing. However, for short shafts of large diameter, shear deflection can have a significant effect in the calculation of critical speeds.

The critical speed programs available to the authors had different equations for calculating the shear effects, some of which over-estimated the shear deflection in test cases. The model which is believed to be most accurate is attributed to Timoshenko and has been used by Lund [2]. The transfer equation for deflection due to both bending, M, and shear, V, is

$$X_{n+1} = X_n + \ell_n\theta_n + \frac{\ell n^2}{2EI} M_n + \frac{\ell n^3}{6EI} V_n - \frac{1.33\ell_n}{A_nG} V_n \quad (13)$$

The last term represents the shear deflection effect.

Convergence Criterion

All critical speed programs of the type described here generate numerical elements d_{ij} of the transfer matrix defined by

$$\begin{bmatrix} M_R \\ V_R \end{bmatrix} = \begin{bmatrix} d_{11} & d_{12} \\ d_{21} & d_{22} \end{bmatrix} \begin{bmatrix} \theta_L \\ X_L \end{bmatrix} \quad (14)$$

where M_R and V_R are the moment and shear at the right end of the rotor, respectively, and θ_L and X_L are the displacements at the left end.

The d_{ij} elements are functions of frequency. The object of the computer algorithm is to find the natural frequencies ω which make the determinant $D(\omega)$ of the matrix D_{ij} as close to zero as possible. A criterion for success which is sometimes used is to require $|D| \leq \epsilon$, where ϵ is a small pre-determined value. If the criterion is not satisfied, an improved estimate for the frequency is calculated from a Newton-Raphson scheme, as follows:

$$\omega = \omega_0 - D_0(\omega_0 - \omega_1)/(D_0 - D_1) \quad (15)$$

where ω_0, D_0 are the most recent values for the frequency and the determinant, respectively, ω_1 and D_1 are previous values of frequency and determinant, and ω is the improved estimate for natural frequency.

As D_0 gets smaller, the difference between ω_0 and ω_1 also becomes smaller. However, an acceptable value of D_0 for one rotor, or for one mode, will often produce unacceptable accuracy (in ω) for another rotor or mode.

It was found that a convergence criterion based on $(\omega_0 - \omega_1)$ was much easier to implement and produced much more consistent and accurate results than a criterion based on D_0.

Experimental Methods and Procedures

In making the experimental measurements of natural frequencies for free-free supported shafts and rotors, certain methods and equipment were found to improve the repeatability and precision of the data obtained, as follows.

Rotor Support

The type of the rotor support that was found to work best for measuring free-free frequencies is shown in Figure 5. With the rotor hung horizontally from two long (⅓ of the rotor length or longer) wires or ropes, the vibration excitation was applied in the horizontal plane. The perpendicular (horizontal) stiffness of each wire support is then

$$K_H = W/2\ell \text{ lb/in}, \quad (16)$$

where W is the weight of the rotor and ℓ is the length of each wire support in inches.

To eliminate any doubt about the possible effect of the supports on rotor frequencies, support stiffness values calculated from equation (16) were used in the computer program and the resulting frequencies compared with the zero support stiffness case. In all but one case, the effect of the support ropes was found negligible. The one exception had support ropes shorter than ⅓ of the rotor length.

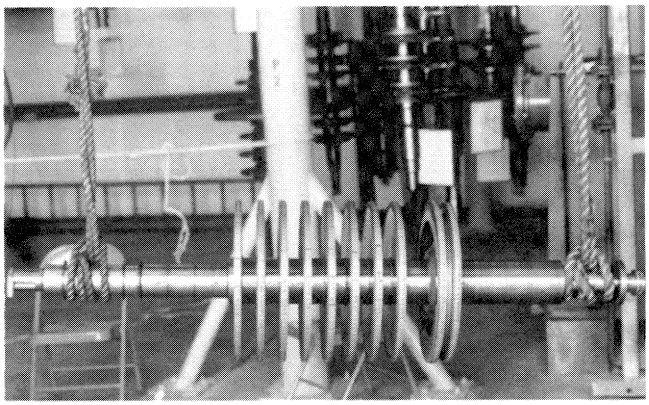

***Figure 5.** Steam Turbine Rotor Suspended by Ropes for Free-Free Vibration Measurements.*

Excitation Methods

Random (white noise), impact (using a rubber or plastic hammer), and to a lesser extent, sinusoidal vibration excitation were all used in the experiments. Random and impact excitations were found to produce comparable results, but the impact method required more time and work on the part of the operator, since a large number of averages were taken. The only disadvantage of the random excitation was that a white noise generator was needed and a suitable shaker had to be attached to the rotor.

The sinusoidal excitation was best suited to cases where only one frequency or mode was investigated, and the signal generator could be tuned to the natural frequency of interest.

Equipment and Instrumentation Used

Experimental data gathering and frequency analysis were greatly facilitated by the use of an HP 5420A digital signal analyzer, with an HP 54470B digital filter and an HP 54410A analog/digital filter. The latter unit contains a white noise signal generator which was frequently used, although a separate Bruel & Kjaer (B&K) random noise generator was occasionally used.

For random or sinusoidal excitation, the excitation signal was amplified by an H. M. Wilson 301 power amplifier, and then fed to a Ling Dynamics shaker model LDS409 attached to the suspended shaft with a stainless steel adjustable hose clamp (Figure 6).

With the single exception of the 3 in uniform shaft, which was measured with proximity probes, the vibration was measured using B&K Type 4344 accelerometers amplified by B&K 2635 charge amplifiers. The accelerometers were very small, weighing 2.7 grams, and had a negligible effect on the natural frequencies of the rotors. The accelerometers were attached to the shaft with machine screws through holes in adjustable stainless steel hose clamps (Figure 6).

Calculated and measured mode shapes were plotted on an HP 9872 plotter, controlled by the HP 9845 computer.

Experimental Techniques

For natural frequency measurements, an accelerometer was mounted on one end of the rotor. It should be noted that

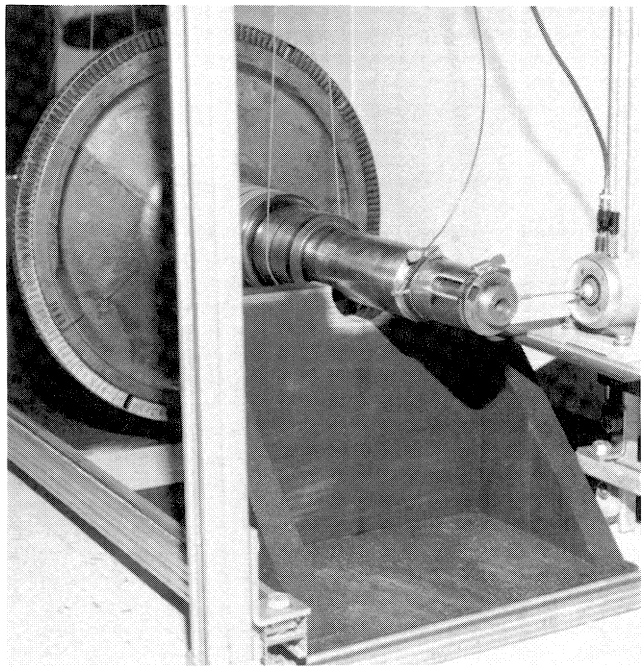

Figure 6. Shaker and Accelerometer Attachment to Shaft.

the rotor end is never a node in free-free vibration. The vibration signal from the accelerometer charge amplifier was input to one channel of the spectrum analyzer, which was preset to the desired number of averages, frequency range of interest, type of excitation, etc. It was found expedient to first produce a spectrum over a broad frequency range, to identify the first four or five natural frequencies, and then to utilize the "zoom expansion" feature of the analyzer to measure each of the identified frequencies with high resolution (small bandwidth). It was found that failure to use a small bandwidth would result in errors up to four percent.

Mode shapes were measured by determining the transfer function between two accelerometers mounted on the rotor. One accelerometer was kept at one end of the rotor as a normalizing input, and the other accelerometer was moved along the rotor to define the mode shape. To maximize confidence in the accuracy and precision of the mode shape measurements, the two accelerometers were calibrated simultaneously on the same clamp, and the coherence function was measured during each transfer magnitude and phase measurement. In almost all of the mode shape measurements, the transfer function phase angle was found to vary less than three degrees from 0° or 180°. This indicated very low damping within the rotor.

The data on rotor dimensions, required to generate accurate computer models, were obtained by making micrometer measurements of the rotor outer diameter (OD) at various axial locations along the shaft (typical spacing between measurements was 2 in) and at all disks and other changes in diameter. These measurements were accurate to within ± 0.001 in. Axial measurements (e.g., the rotor length) were taken with steel rules and were accurate to within $\pm 1/32$ in.

The rotors were weighed, which, together with the dimension measurements, confirmed the weight density of 0.283 lb/in^3 used in the computer models.

Results from Phase I

The measurements described were made on a number of different shafts and rotors, varying in complexity from uniform diametric shafts to an eight-stage centrifugal compressor rotor. The material for all shafts and rotors tested was steel, with Young's modulus taken to be 30×10^6 psi in the computer program. The results are as follows.

Uniform Shafts

A comparison of measured and calculated free-free natural frequencies for two uniform shafts was used to determine the accuracy of the equations and computing procedure used. Since these shafts had only minute changes in station diameter, errors, which are sometimes obtained in modelling rotors having large changes in station diameters, were eliminated.

The measured and computer-predicted natural frequencies for a three inch diameter shaft 50.33 in long are shown in Table 1. The calculated mode shapes for each frequency, with the measured modal deflections plotted as individual points for comparison, are shown in Figure 7.

The measured and computer predicted natural frequencies for a two inch diameter shaft 48 in long are shown in Table 2.

Table 1. Free-Free Natural Frequencies of a Uniform Shaft (three in diameter, × 50.33 in long).

Measured (Hz)	*Computed* (Hz)	*Error* (%)
212.5	213.3	+0.4
581.25	579.9	−0.2
1106.2	1117.6	+1.0
1787.5	1811.9	+1.4
2575	2648.9	+2.9
3731	3612.4	−3.2
	Overall RMS =	1.9%

Table 2. Free-Free Natural Frequencies of a Uniform Shaft (two-in diameter, 48 in long).

Measured (Hz)	*Computed* (Hz)	*Error* (%)
156.05	154.06	−1.3
427.25	418.90	−2.0
827.73	805.53	−2.7
1320.6	1304.22	−1.2
	Overall RMS =	2.5%

The simplicity of this latter shaft, and the uniform magnitude and consistent sign of the error, suggests that most of the error could be due to a slight variation in the value of Young's modulus that was utilized in the computer program. As with the previous shaft, the errors were quite small, with a root mean squared (RMS) average for five modes of only 2.5 percent.

Uniform Shaft – 6 in Diameter, 11½ in Long

The frequencies of a uniform shaft (6 in diameter, 11½ in long) were measured in order to determine the error associated with small length to diameter (L/D) ratios, where shear deflection effects become significant, and where the rule for choosing the number of stations in the transfer matrix model (discussed later) must be modified. Table 3 shows that the effect of direct shear deflection in this shaft is indeed quite significant, changing the RMS error for the first three modes from 2.0 percent

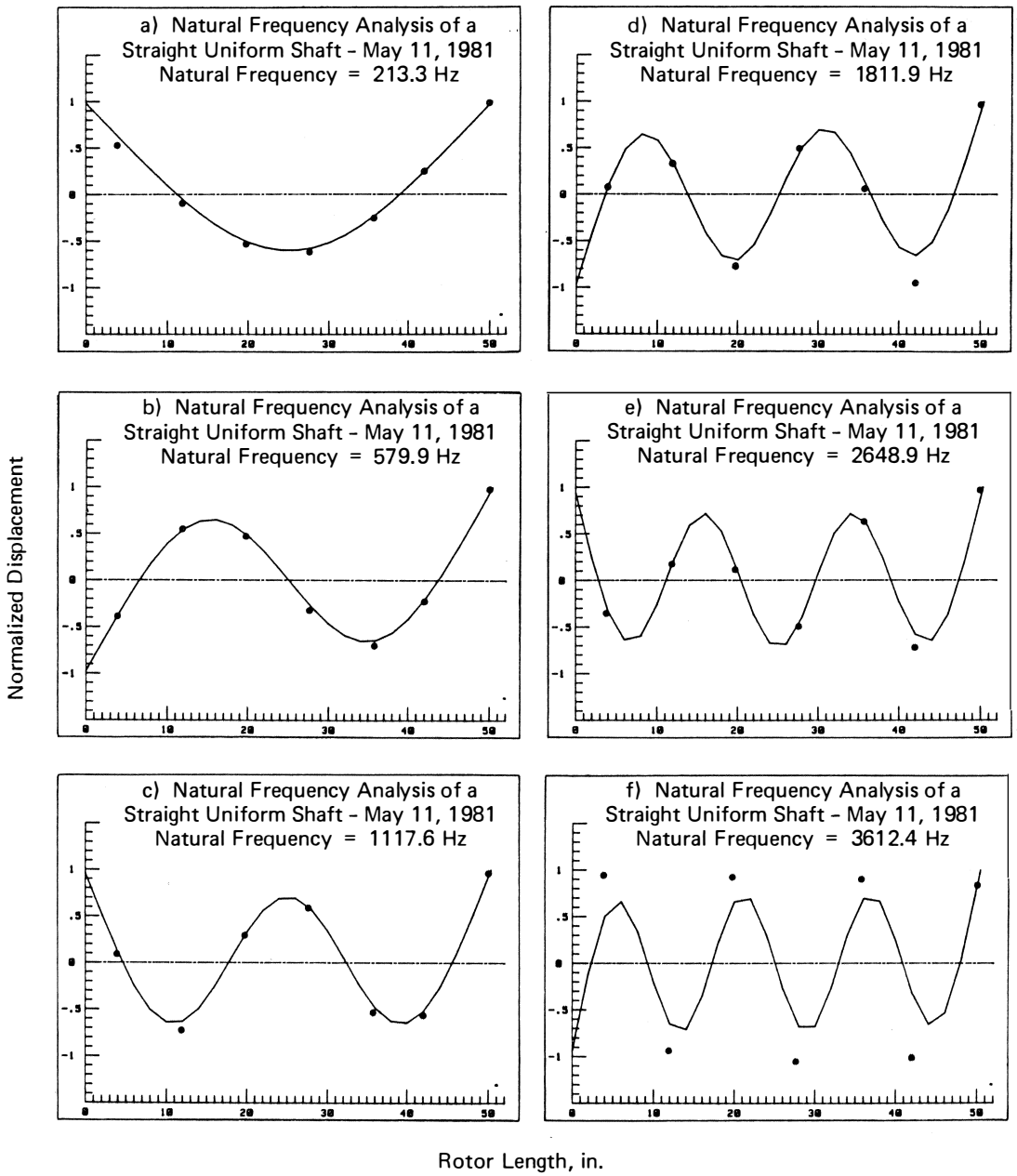

Figure 7. A Comparison of Measured and Calculated Free-Free Mode Shapes of a 3 In Diameter Shaft, 50.33 In Long.

Table 3. Free-Free Natural Frequencies of a Uniform Shaft (Six-inch diameter, eleven and one-half inches long).

Measured	Computed (% error)			
	24 Stations		12 Stations	
Hz	w/shear effect	No shear effect	w/shear effect	No shear effect
5252	5292 (+0.8)	5829 (+11.0)	5593 (+6.5)	6160 (+17.3)
9700	9540 (−1.6)	12947 (+33.5)	9758 (+0.6)	13484 (+39.0)
14489	14063 (−2.9)	21217 (+46.4)	14256 (−1.6)	21828 (+50.7)
Overall RMS Error:	2.0%	33.6%	3.9%	38.3%

(with shear included) to 33.6 percent (without the shear included), when a 24-station model was used. Even with only a 12-station model (four times the number of modes to be computed), the RMS error was less than 4 percent when shear was included.

Some interesting observations were made when making the experimental measurements on this shaft. The frequencies that appeared in the spectrum were quite sensitive to the measurement technique. For example, the natural frequency at 9700 Hz disappeared completely when one particular combination of shaker and random noise generator was used. These types of anomaly were not observed in the measurement on longer shafts and rotors.

Uniform Shaft with a Single Massive Disk

A uniform shaft with a single disk represents one step of complexity away for the uniform shaft. A 9 in diameter, 3 in thick steel disk was hydraulically press-fitted onto a 2 in diameter, 48 3/16 in long steel shaft. A photograph of the assembly is presented in Figure 8.

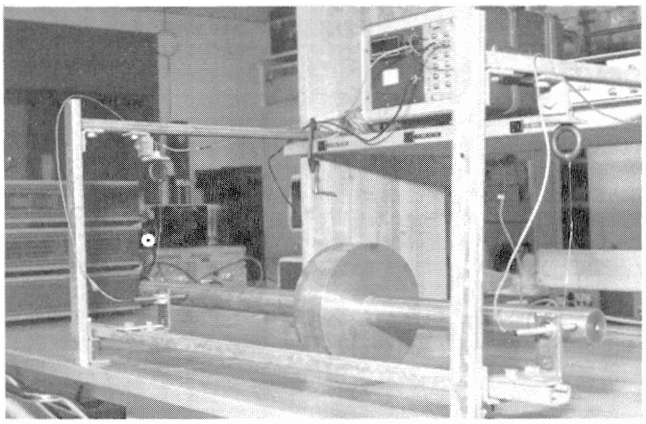

Figure 8. Uniform Shaft with Single Massive Disk.

The first four modes, measured and calculated, along with the error, are given in Table 4. The root mean square error for all four modes was 1.2 percent.

Table 4. Free-Free Natural Frequencies of a Uniform Shaft with a Single Massive Disk.

Measured (Hz)	*Computed* (Hz)	*Error* (%)
130.76	130.45	−0.24
356.64	353.57	−0.86
632.65	632.19	−0.07
1132.80	1157.26	+2.16
	Overall RMS =	1.2%

Three-Disk Laboratory Rotor

A rotor with three disks is the heart of a rotor-bearing test apparatus utilized for rotordynamics research at Shell Westhollow. It has three large disks, but was machined from one piece of stock to eliminate the uncertainty about the effect of attachments or interfaces. The rotor weighs 369.7 lb, and is 52.4 in long. The disks are 9.95 in OD by 5.00 in axial length, and are spaced on 10 in centers. A photograph of this rotor is featured in Figure 9.

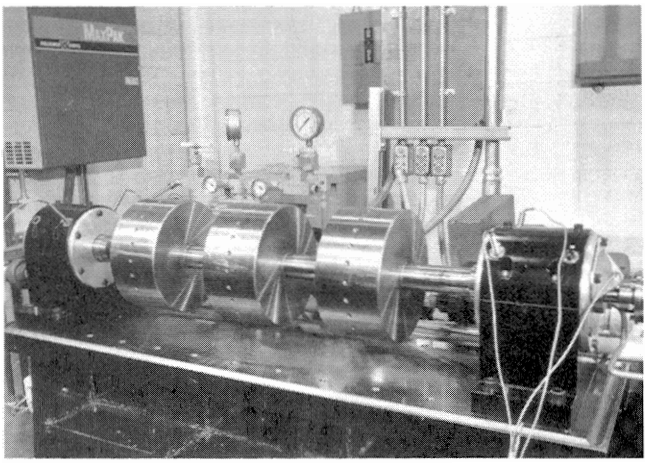

Figure 9. Three-Disk Laboratory Rotor Installed on Tilting-Pad Bearings.

The measured and computed frequencies and the error in percent, both with and without the flexible disk effect included in the computations, are given in Table 5. The attachment stiffness of the 5 in thick disks is so large that the difference between the two results is insignificant. The computed mode shapes for each natural frequency, with the measured modal deflections indicated as individual points for comparison, are shown in Figure 10. The computed mode shapes have the flexible disk effect included.

Table 5. Free-Free Natural Frequencies of a Three-Disk Centritech Lab Rotor.

Measured	Computed	
Hz	No Flexible Disk Hz (% error)	W/Flexible Disk Hz (% error)
94	95 (+1.1)	94 (0)
207	207 (0)	204 (−1.4)
356	353 (−0.8)	350 (−1.7)
463	408 (−11.9)	400 (−13.6)
832	850 (+2.2)	838 (+0.7)
1037	968 (−6.7)	938 (−9.5)
	Overall RMS = 5.7%	Overall RMS = 6.8%

Single-Stage Steam Turbine Rotor

This spare rotor, weighing 262 lb, from a single-stage steam turbine at the Shell Deer Park Refinery was made available to the project for vibration testing. A photograph of the rotor, suspended for free-free tests, is presented in Figure 11.

The rotor is characterized by a turbine disk that is much larger in diameter than the shaft. Not surprisingly, it was found that the disk flexibility effect, described earlier as one of the computer program modifications, was significant in this rotor. Computed frequencies with and without this effect included, in addition to the measured frequencies, are given in Table 6. Note that without the disk flexibility effect, the third measured mode is missed completely.

The computed mode shapes (with the disk flexibility correction) for this rotor are shown as solid lines in Figure 12. The measured modal deflections are plotted as points on the same graph for comparison. Agreement between the results of the

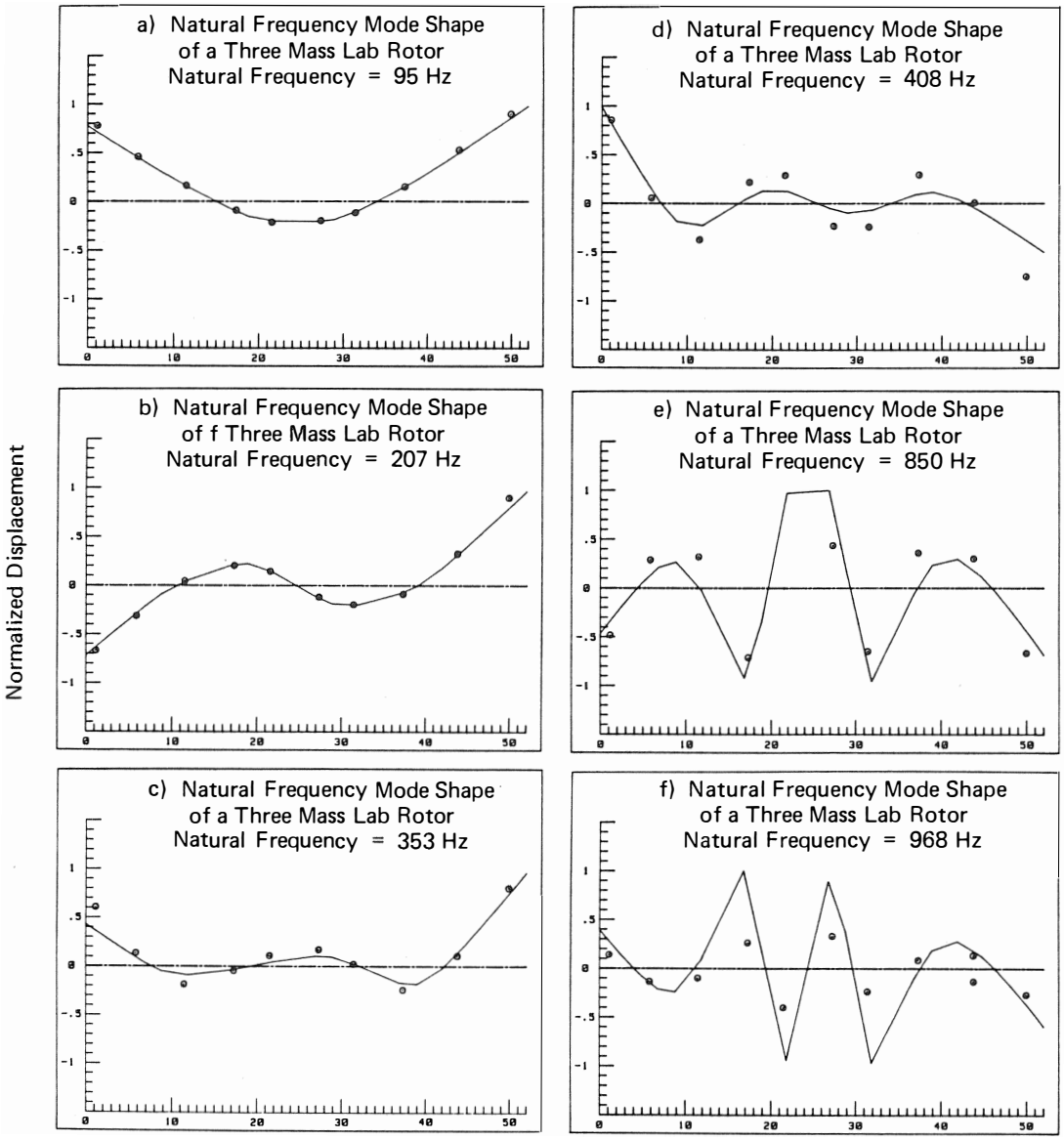

Figure 10. A Comparison of Measured and Calculated Free-Free Mode Shapes of the Three-Disk Lab Rotor.

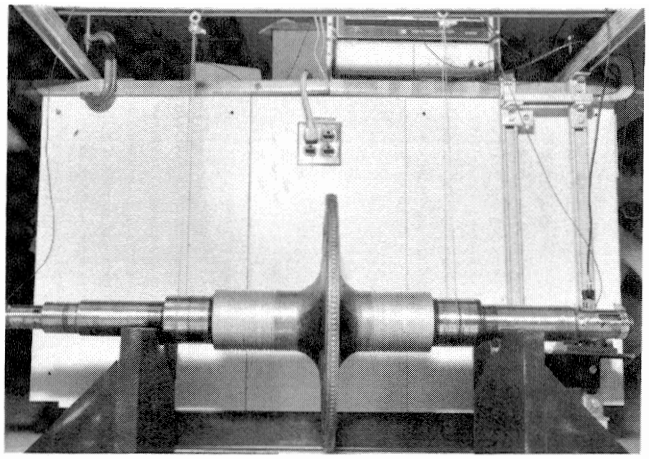

Figure 11. Single-Stage Steam Turbine Rotor, Ready for Free-Free Vibration Measurements.

Table 6. Free-Free Natural Frequencies of a Single-Stage Steam Turbine Rotor.

Measured	Computed	
Hz	No Flexible Disk Hz (% error)	W/Flexible Disk Hz (% error)
373	376 (+0.8)	376 (+0.8)
602	622 (+3.3)	603 (+0.2)
1033	No (∞)	907 (−12.2)
1262	1219 (−3.4)	1230 (−2.5)
1998	1642 (−17.8)	1795 (−10.2)
2509	2321 (−7.5)	2410 (−3.9)
	Overall RMS = 8.9%*	Overall RMS = 6.8%

*Not including Third Mode

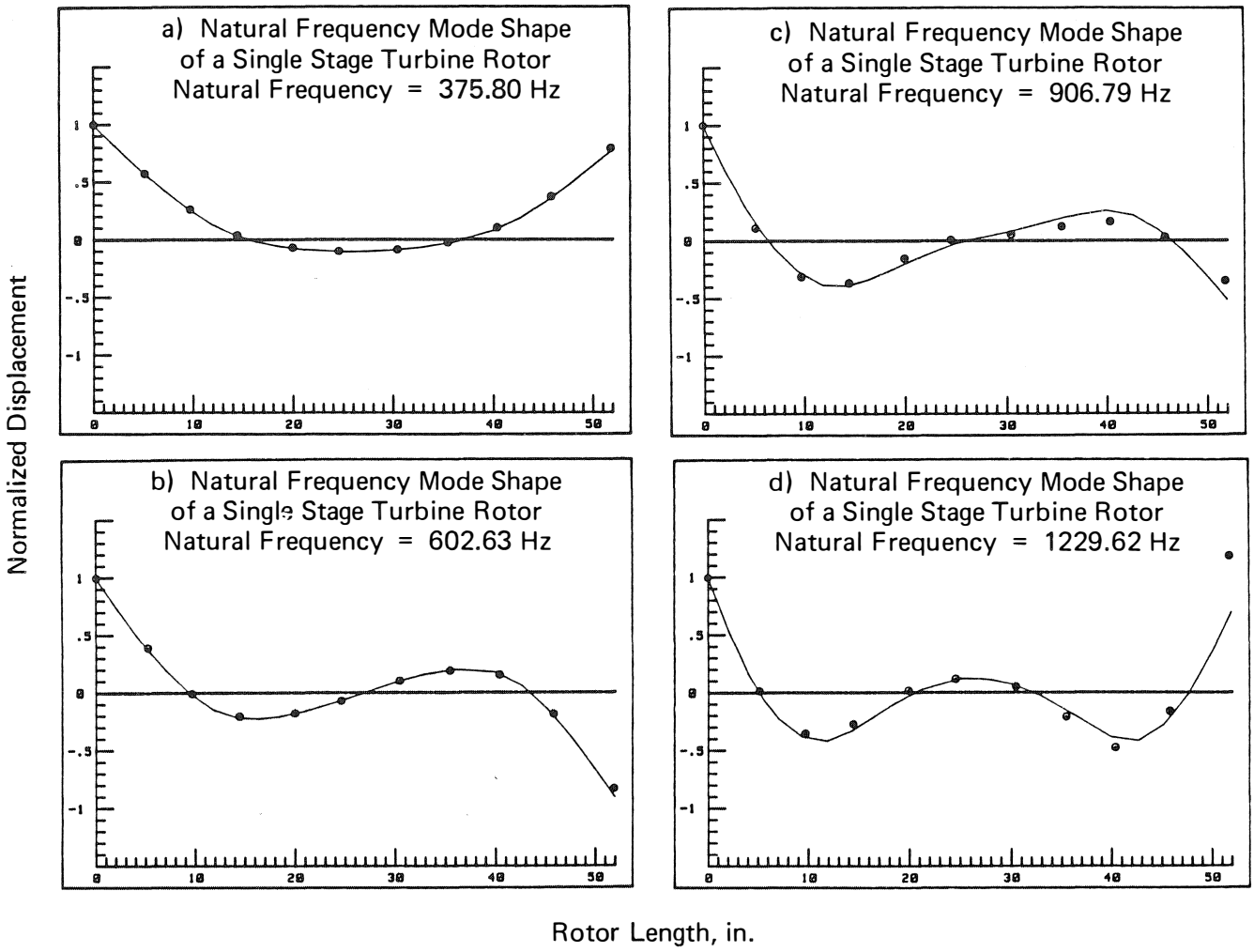

Figure 12. A Comparison of Measured and Calculated Free-Free Mode Shapes for the Single-Stage Steam Turbine.

computer predictions and the experiment was quite good, especially for the first two modes.

Note that both the second and third mode shapes have a node at the turbine disk, and appear very similar. Detailed accelerometer measurements were made on and near the turbine disk to determine the significant differences between the two modes. It was found that the node of the second mode (602 Hz) was located very near the centerline of the disk, and the pitching motion of the disk was in phase with the oscillating slope of the shaft, at the disk location. The node of the third mode (1033 Hz) was located near the inside face of the turbine disk, and the pitching motion of the disk was out of phase with (against) the oscillating slope of the shaft, at the disk location.

The latter mode, in which the disk pitches counter to the motion of the shaft, cannot be computed without the disk flexibility option in the program, which adds an additional degree of freedom to the mathematical model.

Six-Stage Centrifugal Compressor Rotor

This rotor is a replacement for a compressor train at the Shell Deer Park Refinery. It was suspended in a horizontal position by ropes from a crane at the rotor storage facility and excited in the horizontal plane by impact with a nylon hammer. The measured frequency spectrum is shown in Figure 13. Only the first three modes are clearly defined (i.e., is number four a true mode?).

Computed natural frequencies are compared to the measured frequencies for the first three modes in Table 7. Three different cases are presented:

- From rotor station data as supplied by the manufacturer,

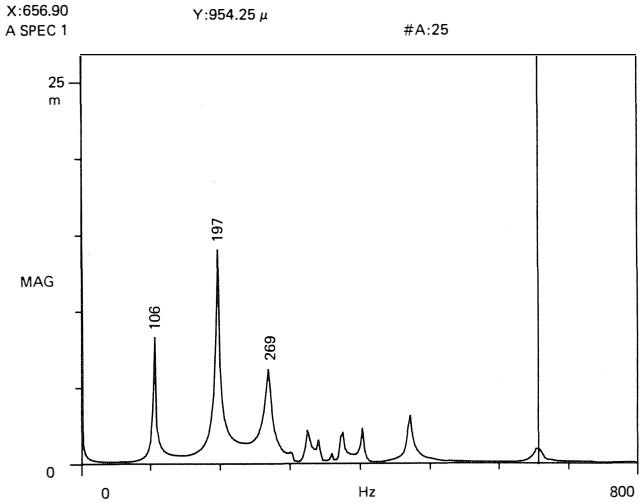

Figure 13. Free-Free Vibration Frequency Spectrum of the Six-Stage Centrifugal Compressor.

• From the manufacturer's data but as modified by actual dimensional measurements, and

• From modified data, and using the "flexible disk" option in the computer program.

The percent error for each case and the overall root mean square error for the three modes is also shown.

The larger errors associated with the first case are due mainly to deficiencies in the rotor data as supplied by the manufacturer. Specifically, both the impeller wheels and the spacer sleeves (between the impellers) are treated simply as added weights in the manufacturers' data. Apparently, the compressor manufacturers' computer program has since been revised to include the stiffening resulting from the sleeves. Information needed for calculating this additional stiffness was not included with the data, and thus was not used in the calculations. Neither the mass moment of inertia of the impellers nor the added shaft stiffness due to the sleeves can be computed from the data supplied. Although these omissions practically cancel their effect on the computed frequency, the net results still indicate an average 12 percent error for the three modes.

To improve the rotor model data, the impeller and sleeve diameters were measured in place on the rotor and used to modify the section diameters accordingly. As shown in Table 7, these modifications reduce the error by a factor of almost two.

The RMS error for case 3 is seen to be misleading when the results for the first two modes (of greatest practical interest) alone are considered.

Eight-Stage Centrifugal Compressor Rotor Number 1

Two eight-stage centrifugal compressor rotors, also spares from the refinery, were investigated. Due to some practical constraints in the storage building, the support ropes and cables were so short in this test that they produced a rigid-body mode of horizontal swinging at 9 Hz. This frequency was high enough to indicate a measureable effect of the supports on the higher modes. Thus, unlike all of the other tests reported herein which the frequencies of the horizontal swing modes were less than 2 Hz, the results for this rotor were affected by the support stiffness.

The measured and computed natural frequencies for the first three modes, along with the errors in percent, are given in Table 8. In contrast to the six-stage rotor, this rotor has the smallest error associated with the third mode when the flexible disk effect is inclued. As in the case of the six-stage rotor, modes above the third mode were not clearly definable on the measured frequency spectrum, even when a logarithmic scale was used.

Eight-Stage Centrifugal Compressor Rotor Number 2

A second eight-stage compressor rotor was obtained and measured in the same manner as the two preceding industrial rotors. The measured spectrum, in which at least the first four modes are clearly definable in terms of their natural frequencies, are shown in Figure 14. A comparison of the computed frequencies with the measured frequencies for the first four modes is shown in Table 9. The three different cases for computed frequencies are defined in exactly the same way as described for the six-stage rotor.

About half of the RMS error shown in the two columns at right in Table 9 can probably be attributed to round-off error in

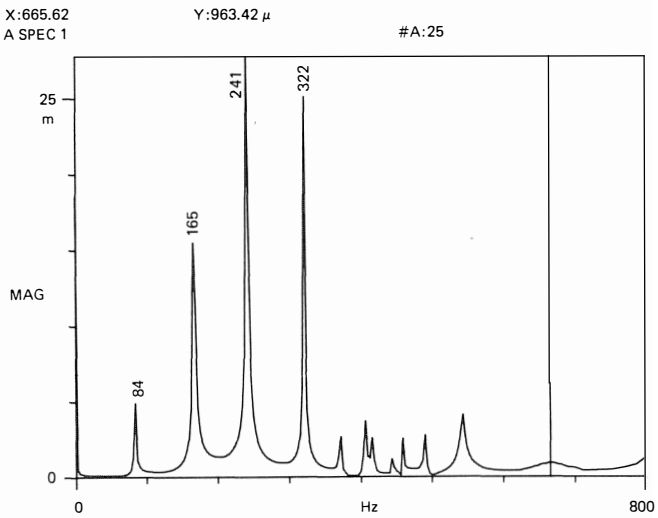

Figure 14. Free-Free Vibration Frequency Spectrum of Eight-Stage Centrifugal Compressor Rotor Number 2.

Table 7. Free-Free Natural Frequencies of Six-Stage Compressor Rotor.

Measured	Computed (% error)		
Hz	from data as received	w/disk I_T and sleeve O.D.s	w/flexible disks
106	87 (−17.9%)	102 (−3.8%)	108 (+1.9%)
197	178 (−9.6%)	192 (−2.5%)	196 (−0.5%)
269	277 (−3.0%)	294 (+9.3%)	303 (+12.6%)
Overall error	RMS = 11.9%	RMS = 6.0%	RMS = 7.4%

Table 8. Free-Free Natural Frequencies of Eight-Stage Compressor Rotor Number 1.

Measured	Computed (% error)		
Hz	from data as received	w/disk I_T and sleeve O.D.s	w/floppy disks
60	39 (−35.0%)	58 (−3.3%)	58 (+3.3%)
142	99 (−30.33%)	130 (−8.5%)	155 (−9.2%)
240	187 (−21.3%)	222 (+7.5%)	243 (+1.3%)
Overall error	RMS = 29.4%	RMS = 6.8%	RMS = 5.7%

Table 9. Free-Free Natural Frequencies of Eight-Stage Compressor Rotor Number 2.

Measured	Computed (% error)		
Hz	from data as received	w/disk I_T and sleeve O.D.s	w/flexible disks
84	69 (−17.9%)	88 (−4.8%)	88 (+4.8%)
165	131 (−20.6%)	173 (−4.8%)	172 (−4.2%)
241	178 (−26.1%)	267 (+10.8%)	267 (+10.8%)
322	264 (−18.0%)	382 (+18.6%)	404 (+20.3%)
Overall error	RMS = 20.9%	RMS = 11.3%	RMS = 11.9%

the computer. The same mass-elastic model on a different computer (HP 9836) indicated an average error for the four modes of only 5.33 percent.

13-Stage Steam Turbine Rotor

A steam turbine rotor with 13 stages, used in the same train with the previously described compressors, was also tested in the same way as previously described. The measured frequency spectrum, in which at least the first four modes are readily definable, is shown in Figure 15. The computed and measured frequencies are compared in Table 10. There are only two cases under the "computed" heading for this rotor, either with a rigid or a flexible attachment of the disk to the shaft. The rotor data, as supplied by the manufacturer, included all of the actual outside diameters of the wheels and shaft sections.

Table 10. Free-Free Natural Frequencies of Delaval 13-Stage Steam Turbine Rotor.

Measured	Computed (% error)	
Hz	w/rigid disks	w/flexible disks
141	135 (−4.3%)	135 (−4.3%)
284	297 (+4.6%)	289 (+1.8%)
388	454 (+17.0%)	309 (−20.4%)
509	612 (+20.2%)	425 (−16.5%)
Overall Error	RMS = 13.6%	RMS = 13.3%

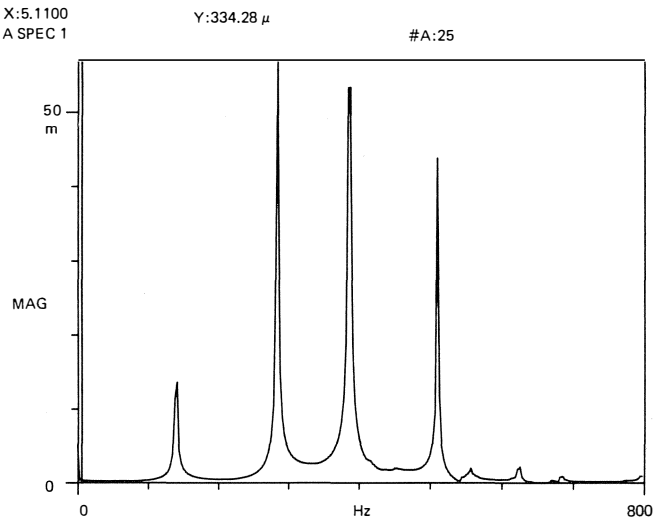

Figure 15. Free-Free Vibration Frequency Spectrum of the 13-Stage Steam Turbine Rotor.

If only the first two modes are of practical interest, the flexible disk computer model is more attractive, since it produces the same error for the first mode, but reduces the error by approximately 50 percent for the second mode.

Rules for Computer Modelling of Shafts and Rotors

Some rules and guidelines which were found to produce optimum accuracy as determined by comparison against careful experimental measurements have been developed. Since the computer programs used in this study were based on the transfer matrix method, with lumped masses and inertias, the rules and guidelines should be used only for these types of programs. The guidelines developed are as follows:

- The optimum length of shaft used for each station is the maximum diameter in the station. Using additional shorter stations does not increase the program accuracy. Furthermore, the number of stations must be at least four times the number of desired modes to be computed.
- Wherever disks, wheels, or sleeves are present on the shaft (even if pressed on or keyed), the disk or sleeve outside diameter should be used in calculating the bending stiffness of the section.

Whenever disks or wheels of diameter more than twice the shaft diameter are located near a node of a particular mode of natural vibration, the flexible disk effect is likely to be significant and should be included in the model. This will split the computed frequency into two natural frequencies, one below and one above the frequency for a rigid disk attachment.

PHASE II: ROTOR-BEARING SYSTEMS

Computer Program

As mentioned under Phase I, a transfer matrix program with damping included was written to compute the damped critical speeds of rotor-bearing systems. In addition to damping, the program includes the effects of internal friction, bearing asymmetry, and cross-coupling from bearings, seals, or fluid forces around impellers, as well as foundation impedance effects. The output from the program consists of complex eigenvalues and eigenvectors (mode shapes). Thus, in addition to damped critical speeds, the program computes nonsynchronous whirl frequencies with their corresponding logarithmic decrements. The latter is a measure of the margin of rotordynamic stability.

The algorithm is based on a method of eigenvalue calculation set forth in a previous paper by Murphy and Vance [7]. Using this method, only one pass through the transfer matrices is required to generate the characteristic polynomial for the system. A rootfinder subroutine is then used to find the complex eigenvalues. Unlike some of the programs based on the Lund algorithm [2], convergence is always obtained and no critical speeds are missed. Computation times are also reduced, usually at least by a factor of one half.

The new program, named "JAZZ," was implemented on an HP 9836 desktop computer in Series 200 Extended Basic. System modelling of the rotor is performed in the same manner as for any transfer matrix program. The refinements described previously were also incorporated into the program.

Experimental Measurement of Tilt-Pad Bearing Properties

The primary objective of the work on rotor-bearing systems was to assess the accuracy of predicting critical speeds for a rotor supported in fluid-film bearings. The critical speeds of a machine are greatly influenced by the stiffness and damping properties of the bearings. In general, the properties of fluid-film bearings are a function of the operating conditions, including shaft speed and bearing load. Tilting-pad bearings are often used on high speed turbomachinery because of their favorable influence on rotordynamic stability. Very little experimental work has been published to verify the extensive analytical work which has been published for this type of bearing. Two of the rotors selected for this study were supported on 5-pad tilting-pad bearings when in operation. Therefore, the operating characteristics of these bearings were measured so relevant comparisons could be made of predicted and measured critical speeds.

Description of Test Apparatus for Tilt-Pad Bearings

The apparatus used for measuring the bearing characteristics is based on a piece of equipment that was originally built for modelling the vibration characteristics of turbomachinery rotors. As shown in Figure 16, the apparatus consists of a 50.5 in uniform rotor, 2.5 in diameter, supported by 5-pad tilting-pad bearings mounted near each end of the shaft. The outboard bearing is used as the test bearing. A photograph of the test bearing and its loading mechanism is shown in Figure 17.

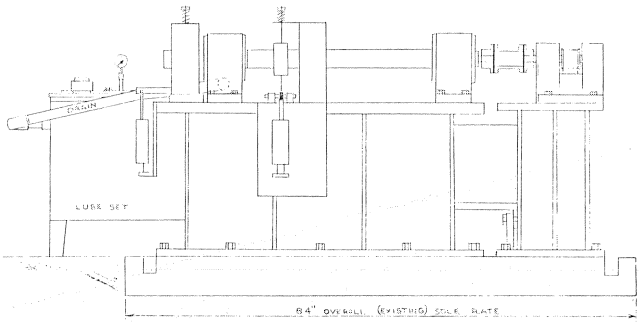

Figure 16. Rotor-Bearing Test Apparatus.

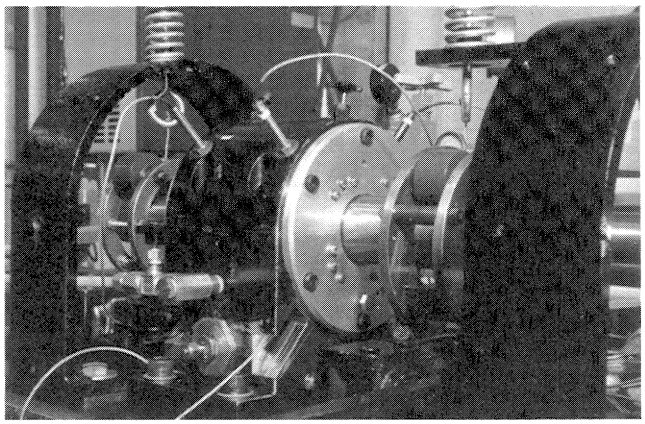

Figure 17. Test Bearing and Load Mechanism.

The two bearings used in this study were manufactured specifically for this test rig and were adjusted to have the following specifications:

load on pad
L = 1.0 in
D = 2.504 in
arc length = 60 degrees
radial clearance = 0.002 in
preload = 0
viscosity = 3.3 μreyns at 100°F (SAE 10)

Since thermal expansion during the tests was expected to result in slightly different bearing clearances, actual clearances were measured following each test.

The bearing pads had spherical seats that were mounted in mating seats in the bearing housing to accommodate angular misalignment with the shaft. The rotor was driven through a flexible coupling by a 30 hp variable speed electric motor.

The uniform shaft had a total weight of 75 lbs. This resulted in a journal load of 41.5 lbs at the test bearing. This shaft was later replaced with a 3-inertia rotor for the critical speed study. Additional external loads were applied vertically to the test bearing through pairs of plastic rollers running on the shaft inboard and outboard of the test bearing as shown in Figure 18. The rollers were mounted in a yoke, which was acted upon by low friction air cylinders. Lever arms connecting the air cylinder to the yokes were adjustable, so an equal bearing load could be applied by each yoke for the same air pressure. Small horizontal loads were also independently applied to the test bearing by a simple system of weights and pulleys attached directly to the sides of the yokes. The applied horizontal load could not exceed one-half of the applied vertical load without disrupting the loading system.

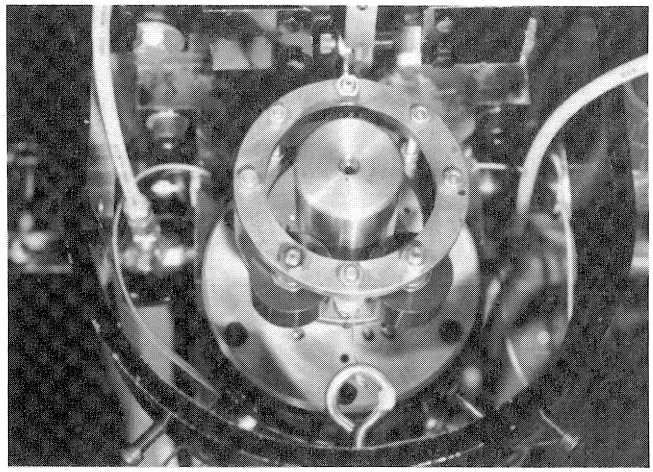

Figure 18. Outboard Yoke and Rollers on Test Bearing.

The shaft location within the bearing was measured using eight non-contact eddy current proximity probes, mounted in orthogonal pairs 0.75 in from each end of the test bearing. Static shaft positions were obtained by using low-pass filters to remove the dynamic component of the probe signals, leaving only the static position. Measurements from probes radially opposite each other were combined so that the average difference between the probes gave the relative shaft position with respect to the probe tips, while cancelling the effect of uniform thermal expansion of the shaft and bearing housing. Averaging of the data at both ends of the bearing was used to determine the shaft position at the mid-point of the bearing.

The oil temperature was monitored at the bearing inlet, in the oil bath surrounding the bearing pads, and at the oil exit from the bearing. The actual bearing pad temperature was monitored with a thermocouple in one of the two test bearings. The oil temperature was controlled to a limited degree by using valves to control the flowrate of oil to the test bearing.

All data was recorded on a computerized data acquisition system.

Vertical Stiffness Measurements

Vertical loads were applied to the bearing through the air cylinders, and the resulting shaft deflections were measured [8]. A trace of the shaft center's downward movement (i.e., the static load curve) as the load is slowly increased is shown in Figure 19. The path is seen to be smooth with about a ten percent slope off the vertical. Theoretically, a tilting-pad bearing has no cross-coupling and the path should, therefore, be straight down. A cross-coupled stiffness that is always ten percent of the direct stiffness would cause the observed path to be followed. From the 100 data points taken, each increment in load was divided by each increment in displacement to obtain the stiffness.

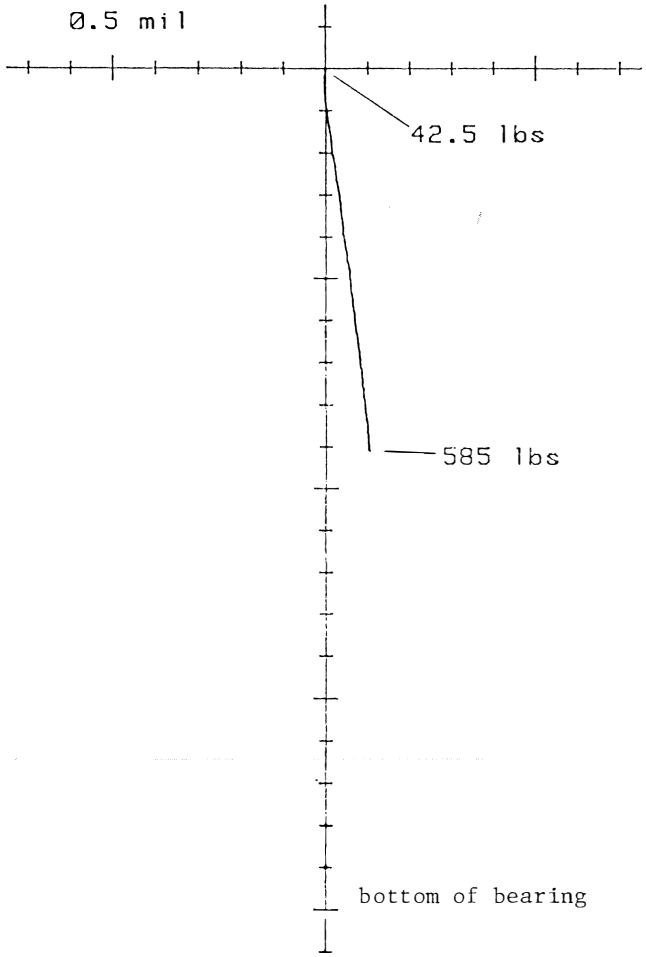

Figure 19. Static Load Curve for Tilt-Pad Bearing.

The vertical stiffness values (K_{yy}) obtained at the speed-load-temperature combinations indicated are presented in Table 11. Each stiffness value shown is the average of all data taken at that set of conditions.

Horizontal Stiffness Measurements

The side load apparatus described earlier was used as a means of measuring the horizontal bearing stiffness. For a chosen set of operating conditions (speed-load-temperature), small increments in horizontal load were applied using the weights and pulleys, and the resulting increments in deflection were recorded. All values are shown in Table 11 as K_{xx}.

The measured horizontal stiffnesses K_{xx} were found to be larger than the measured vertical stiffnesses by as much as a factor of three. The direction of major load (from the air cylinders) was vertical.

Experimental Identification of Critical Speeds

A variety of methods can be employed to measure the critical speeds of a rotor-bearing system. The choice of method is usually constrained by practical or economic considerations when the measurement is to be made on an operational industrial machine. To eliminate these constraints and allow a number of different methods to be tried, a rotor-bearing system was constructed at the Shell Westhollow Laboratories. The rotor (Three-Disk Lab Rotor) and the tilt-pad bearings have been described in previous sections, and will be henceforth referred to simply as the lab rotor.

Startups and Shutdowns

The most widely used method for measuring critical speeds is done during a startup or shutdown. The vibration signal for any suitable pickup can be fed through a synchronous tracking filter allowing a plot of synchronous vibration as a function of running speed. The critical speeds are then identified by the peaks on this plot. Another effective way of obtaining the same plot is to input the unfiltered signal into a Fast Fourier Transform (FFT) analyzer set on peak hold. For the lab rotor, the FFT plot for coastdown through the first critical speed of 30.5 Hz (1830 rpm) is presented in Figure 20. Coastdown through the second, third and fourth critical speeds of 108 Hz (6480 rpm), 126 Hz (7560 rpm) and 155 Hz (9300 rpm), respectively, is shown in Figure 21. The logarithmic decrements were obtained from these plots by using the half-power point method [9].

Table 11. Measured Stiffness Values for Tilt-Pad Bearing.

Shaft Speed (rpm)	Bearing Load (lbs)	Kxx (lb/in)	Kxy (lb/in)	Kyx (lb/in)	Kyy (lb/in)
1500	185	620000	62000	59200	592000
1800	185	606000	60600	49700	497000
2200	185	704000	70400	34000	340000
4000	185	853000	85300	42400	424000
4000	92.5	679000	67900	22400	224000

It should be remembered that one drawback of this method of determining the critical speeds of the rotor in the field is that closely spaced critical speeds, such as those shown in Figure 21, may appear as a single, heavily-damped, critical speed, if the startup or shutdown happens too rapidly.

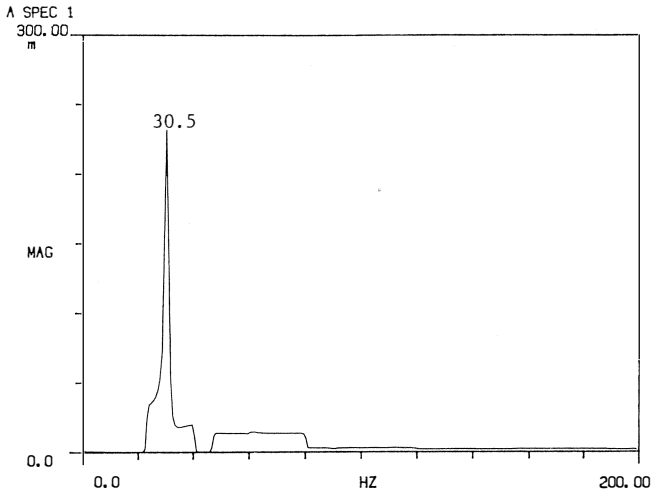

Figure 20. Lab Rotor Vibration during Coastdown through First Critical Speed.

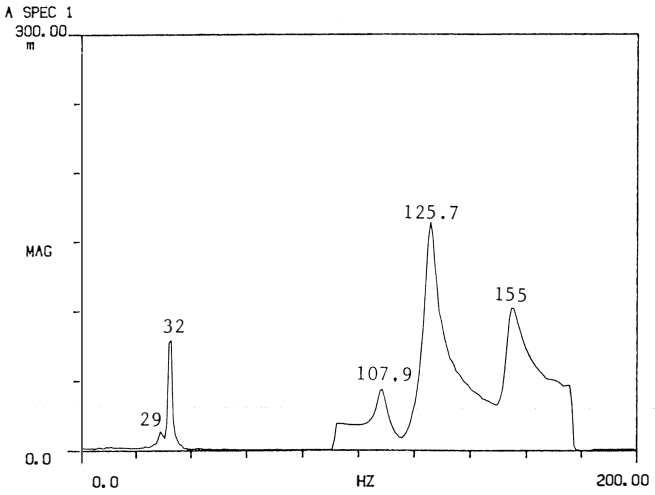

Figure 21. Lab Rotor Vibration during Coastdown through Fourth, Third, and Second Critical Speeds.

Second Harmonic of Running Speed

The first method discussed for determining the critical speeds was based on the synchronous response (running speed spike on the spectrum) reaching a peak while passing through a critical speed. A possible alternative to using the synchronous response would be to use its second harmonic, or a frequency equal to twice the running speed. On a frequency spectrum the running speed spike is almost always accompanied by its second harmonic (Figure 22), and it was thought possible that this spike may also reach a peak while passing through a critical speed. This could allow identification of critical speed frequencies up to twice the maximum operating speed.

This approach was tried on the lab rotor without success. When the second harmonic of the running speed passed through the known critical speeds, no peaks were observed.

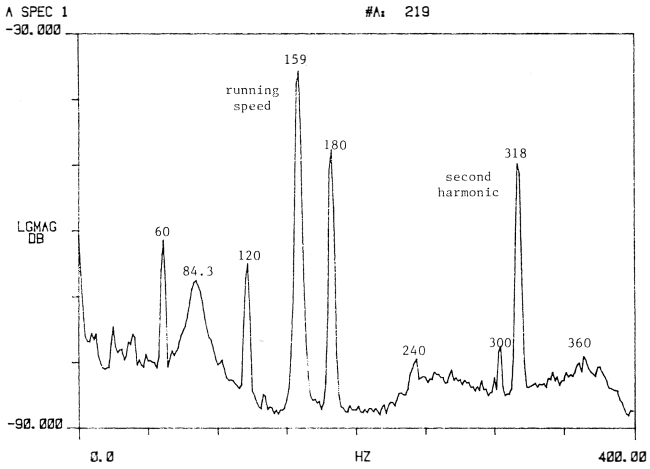

Figure 22. Vibration Spectrum Showing Running Speed Component with its Second Harmonic.

Impact on Shaft or Bearing Housing

In the field, machines often run at a constant speed which cannot be varied. For this reason, it is desirable to have some means of identifying critical speeds from measurements made at a single speed. For this to be possible, there must be some source of vibratory excitation at each of the critical speeds so that they may be identified by a frequency spectrum plot. One way to get this excitation is by impact with a rubber or plastic hammer on either the rotating shaft itself or on the bearing housing and/or support.

For the lab rotor both these methods were tried and both worked satisfactorily. The types of spectrums obtained are shown in Figures 23 and 24. In the field, though, it is usually not possible to impact the shaft directly. Thus, an important result is that impact on the bearing housing worked as well as, if not better than, impact on the shaft.

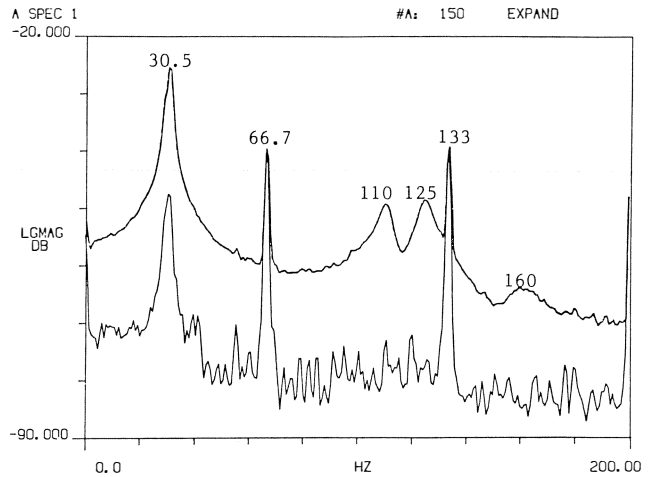

Figure 23. Before and After Vibration Spectra for Hammer Blows on the Lab Rotor Shaft at 4000 RPM.

Shaker Attached to Housing

Another method that was tried on the lab rotor, with the shaft running at constant speed, was to connect a 25 lb shaker to one of the bearing housings. This method was not found to work satisfactorily with the shaft running at high speeds. The use of a larger shaker might have provided better results, but was not available.

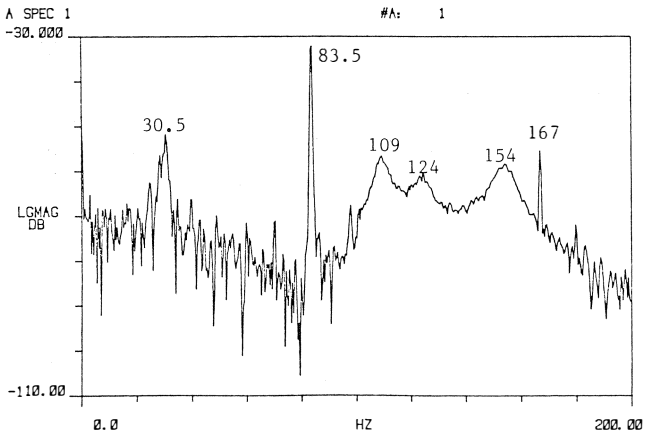

Figure 24. Vibration Spectrum for a Hammer Blow on the Lab Rotor Bearing Housing at 5000 RPM.

Incipient Surge

Another possible way to get the required vibratory excitation on some compressor trains is by causing the machine to surge. When surge occurs the entire system is severely "impacted" by the working fluid within the machine. To investigate this, the vibration spectrum of a single-stage turbine driving a process compressor in the region of surge was chosen. The vibration spectrum of the turbine while operating at 9500 rpm (158 Hz) is shown in Figure 25. The synchronous vibration at 158 Hz is not necessarily a critical speed, although its large amplitude suggests the possibility. Its first harmonic is at 318 Hz. Electrical noise at 60 Hz and all its harmonics must be eliminated. The most likely critical speeds are therefore 140 Hz, 205 Hz and 219 Hz, with a possible critical speed near 158 Hz. This partially corresponds with past experience with this turbine since startup information indicates that the machine goes through one critical speed around 8000 rpm (133 Hz) and approaches another critical speed at its top speed of around 11,000 rpm (183 Hz). Another spectrum, taken at a later time, shows the spike at about 200 Hz more clearly with the spike near 220 Hz much less noticeable (Figure 26). For later comparisons with the computer program, the critical speeds of the single-stage steam turbine will be assumed as 140 Hz and 205 Hz.

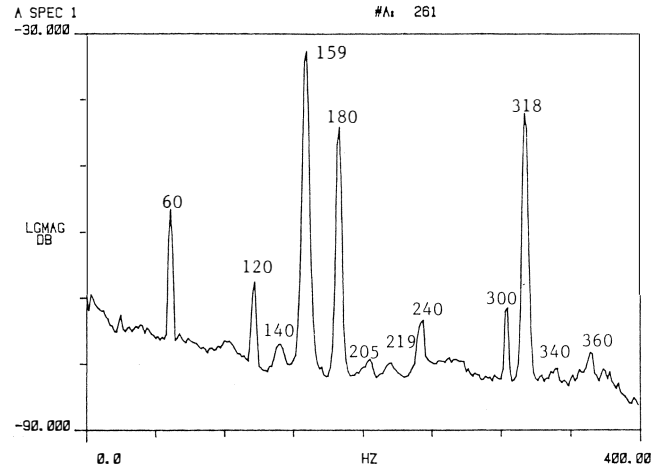

Figure 25. Vibration Spectrum for the Single-Stage Steam Turbine Running at 9500 RPM.

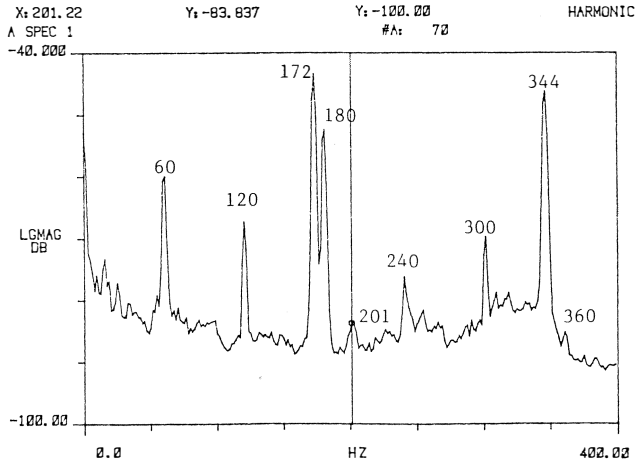

Figure 26. Steam Turbine Vibration Spectrum with 200 Hz Component More Pronounced.

Backward Whirl Modes

Due mainly to the effect of support asymmetry and gyroscopics, backward whirl modes may be present in turbomachinery. Backward modes are usually not considered in a critical speed analysis, because it has been generally believed that they cannot be excited by rotor unbalance. The lab rotor provided a good example of a backward whirl mode. The frequency spectrum obtained during coastdown through the second, third and fourth critical speeds is shown on Figure 21. The two spikes at the first critical speed are in the form of subsynchronous whirling. The short spike at 29 Hz is the backward component of the first mode. The spike at 32 Hz is the forward component and would normally be called the first critical speed. It would be difficult, at best, to interpret this from an orbit displayed on an oscilloscope screen. However, the same two displacement probes normally used to display an orbit were fed into a two channel FFT analyzer. The transfer function (Figure 27) of one signal divided by the other indicated the whirl direction. At a frequency of 32 Hz the signal from probe two led the signal from probe one by 90 degrees, indicating forward whirl. At 29 Hz the signal from probe two lagged the probe one signal by 90 degrees, indicating backward whirl at this frequency.

The phase angle at the other three critical speeds were seen to be either 0 or +180 degrees. This indicated modes that are very close to being planar modes (i.e., the orbit is a straight line). The actual whirl directions of these modes are not particularly important because they are so very nearly planar. The forward rotating unbalance force can excite them regardless of their respective whirl directions. In actuality, the orbital directions of such planar modes could be different at different axial locations along the rotor.

Machine Foundations

The three closely spaced critical speeds that were measured for the lab rotor clearly indicated that the rotor response was being strongly influenced by the test rig foundation. For an accurate computer simulation to be possible, this effect must therefore be included. The computer program that was developed permitted any bearing(s) to be mounted on a foundation mass which in turn is supported by a linear spring and damper combination. The model is presented in Figure 28. Different foundation parameters can be specified for each bearing, and for each bearing different parameters can be specified for the horizontal and vertical directions. Note that one limitation inherent in this type of foundation model is that

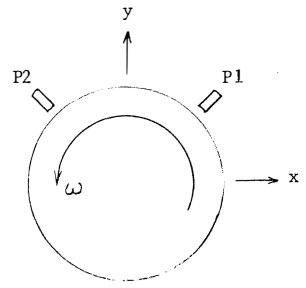

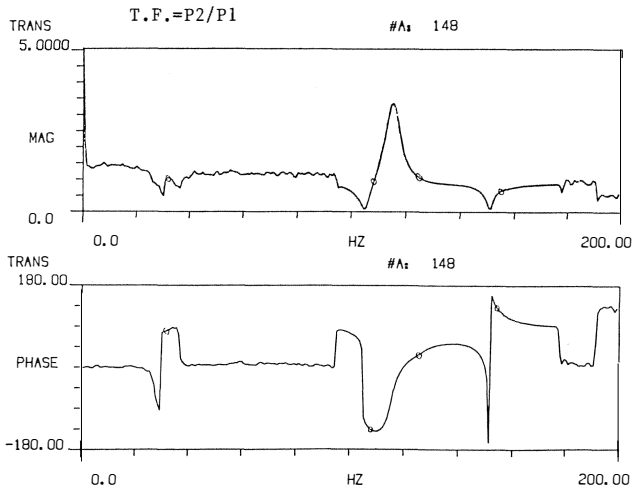

Figure 27. Transfer Function of Probe P2 Signal to Probe P1 Signal.

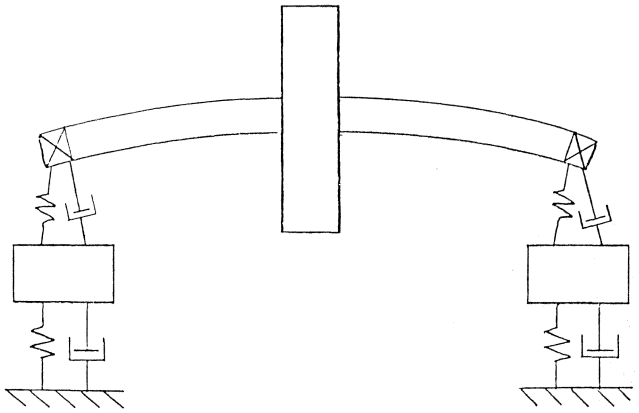

Figure 28. Single-Mass Model for Bearing Impedance at Each Bearing.

there is no direct coupling between the various foundation masses. The best way to obtain numerical estimates for the foundation parameters is from impedance measurements made directly on the foundation when the rotor has been removed.

Measurement of Foundation Parameters

The foundation parameters are readily obtained from driving point impedance measurements made directly on the bearing housing. With a predetermined harmonic force applied to the structure by use of a shaker, the response of the structure is measured with an accelerometer or velocity pickup. Mechanical impedance is defined as the ratio of the applied force (magnitude and phase) to the measured velocity (magnitude and phase). Should the shaker and velocity pickup be at the same location, then the result is termed driving point impedance. A shaker connected to an idealized foundation model through a force transducer, with a velocity pickup or an accelerometer with an integrated signal as was used on the lab rotor mounted next to the force transducer is shown in Figure 29. The measurement procedure used was to drive the shaker with a random noise signal and record the force and acceleration on a magnetic tape recorder for later analysis. Using a random noise signal allows the measurements to be taken for all frequencies simultaneously. Analysis of the recorded data is performed with a two channel frequency analyzer that permits integration and differentiation of the signals, as well as computing the transfer functions. The analyzer displays that would be obtained for the ideal one degree-of-freedom foundation shown are also featured in Figure 29. The foundation stiffness is obtained from the $\dot{X}/F$ curve by reading the value where the frequency approaches zero, and taking its reciprocal. The stiffness associated with all higher natural frequencies must be rigid in comparison with the fundamental stiffness being measured here. Foundation damping is obtained from the $\dot{X}/F$ curve by reading the value at the peak (i.e., at the natural frequency), and taking its reciprocal ($C = F/\dot{X}$). Foundation mass is then calculated from the expression $\omega^2 = K/m$ with the frequency and stiffness known.

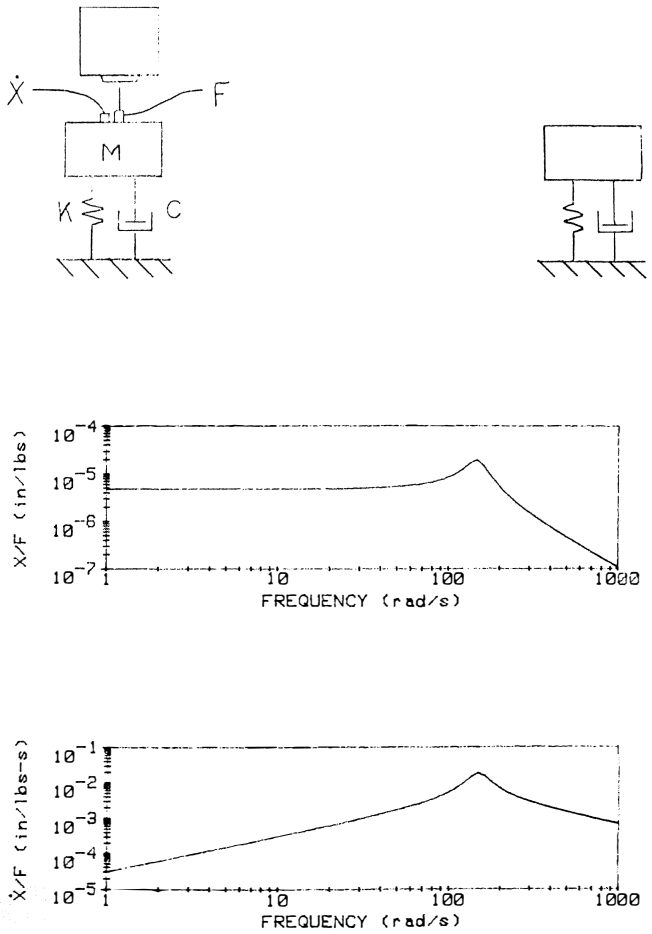

Figure 29. Shaker Attachment to Foundation and the Resulting FFT Analyzer Displays (for idealized case).

For the lab rotor, some simple rap tests using a hammer were used to check the natural frequencies of the foundation. It was found that the structure had a horizontal mode around 149 Hz. Vertically, the sructure was found to be essentially rigid with a fundamental frequency in excess of 300 Hz. Measurements were therefore made horizontally only, and were made on just one housing due to the symmetry of the structure. The plots obtained from the frequency analyzer are shown in Figure 30. The parameters calculated are as follows:

frequency = 149 Hz
stiffness = 208,000 lbf/in
damping = 55.6 lbf-s/in
mass = 92.0 lbm

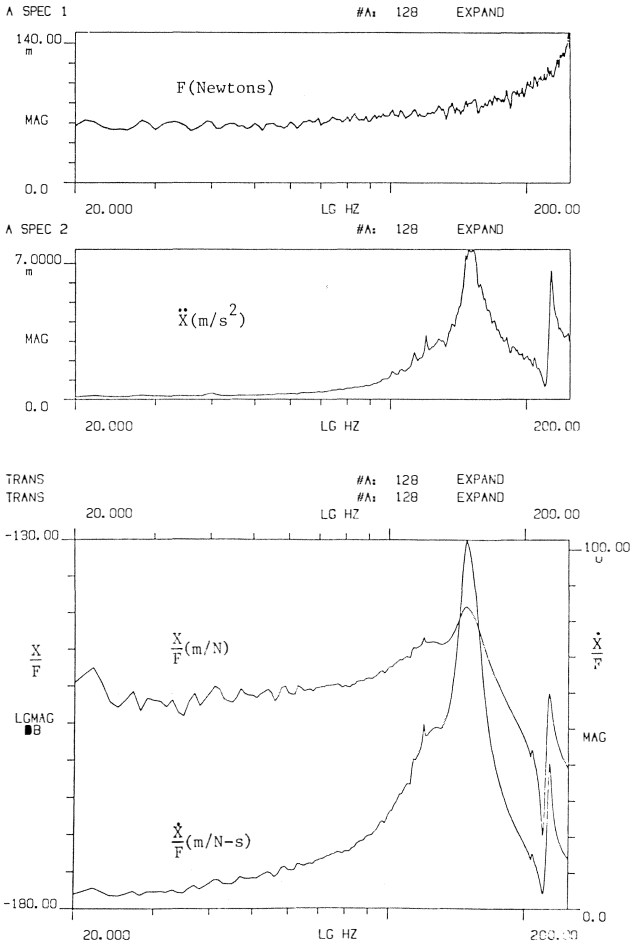

Figure 30. Measured Impedance Functions for the Outboard Foundation of the Lab Rotor Test Rig.

Foundation Measurements with Shaft in Place

It is recommended that the rotor be removed from the machine when making foundation measurements. In cases where this is not practical, it still may be possible to obtain the desired parameter values from impedance measurements. If the presence of the shaft does not affect the stiffness of its supporting structure, as would almost certainly be the case, then the foundation stiffness can be measured as before. After obtaining the stiffness, an estimate of the mass is obtained from $m = K/\omega^2$. The mass value calculated has been shown to be correct as long as the rotor does not significantly alter the measured natural frequency of the foundation, but at this point it is not known whether or not this is true. If the mass of the rotor is much lighter than the calculated mass, it should be safe to neglect it. If possible, the calculated first and second rigid bearing criticals should be compared to the measured foundation frequency. If either is in the same ballpark as the foundation frequency, then splitting of modes will almost certainly occur and this will cause two peaks on the measured response curve instead of one. This was the case with the lab rotor. The separation between the peaks will increase with increasing rotor mass. Using a frequency midway between these two values could then be used as the foundation requency. Some more complex analytical methods may also be used to correct for the presence of the rotor.

The measurement of damping is performed as described before when the rotor is light. If the rotor is not light but can be considered rigid (high rigid bearing criticals) at the measured frequency, then the damping constant is also obtained as before. If there is splitting of the mode since the rotor is neither light nor rigid, then using the peak at the lower frequency to obtain the damping constant should yield a conservative estimate. A more complex analytical method may again be used to correct for the presence of the rotor.

Foundation Measurements with Rotating Shaft

It is desirable to be able to measure the foundation's characteristics not only when the rotor is present, but while it is running at its operating speed. For this to be possible, all the considerations of the preceding section must be observed. In addition, the steady state vibration signature of the machine must also be dealt with. Force and response measurements should be recorded both before and after activating the shaker. The foundation parameters were shown to be obtained from the transfer function plots at certain frequencies, therefore at these frequencies the values from the machine's signature transfer function must be insignificant compared to those obtained with the shaker running.

This method was tried on the lab rest rig. Good results were obtained at 1000 rpm, but at 5000 rpm the vibration signature was too large. A larger shaker (i.e., more force) may have provided better results at this higher speed.

Subsynchronous Whirling of the Lab Rotor

All test measurements performed on the lab rotor were done with the rotor running on 5-pad tilting-pad bearings as described earlier. The test environment had the rotor spinning in free air. It should also be noted that the test rotor is one solid piece of steel, having been machined from a single piece of stock. Under these conditions no subsynchronous whirling should be expected on the test rig, since there is no known source of excitation. The steady state vibration spectrum obtained with the rotor running at a constant speed of 9300 rpm (155 Hz) is shown in Figure 31. An extremely large subsynchronous component of vibration is clearly evident at the first critical speed of 32.4 Hz. Also note the presence of the backward whirl mode at approximately 30.5 Hz. This subsynchronous vibration was present in varying amounts for shaft speeds from about 3500 rpm up to the maximum attainable speed of 10,500 rpm, but at no other shaft speed was it as high as it was at the fourth critical speed of 9300 rpm (155 Hz). The whirl frequency ratio is seen to be 4.78 to one, or approximately 20 percent. During coastdown, the maximum subsynchronous amplitude occured at a speed just above the fourth critical speed at a frequency of 156.7 Hz (Figure 32). Note that it is not quite as high as it was at steady state, but that the whirl ratio is still 4.78 to one.

An attempt was made to measure the logarithmic decrement of the subsynchronous whirl mode using the method of a

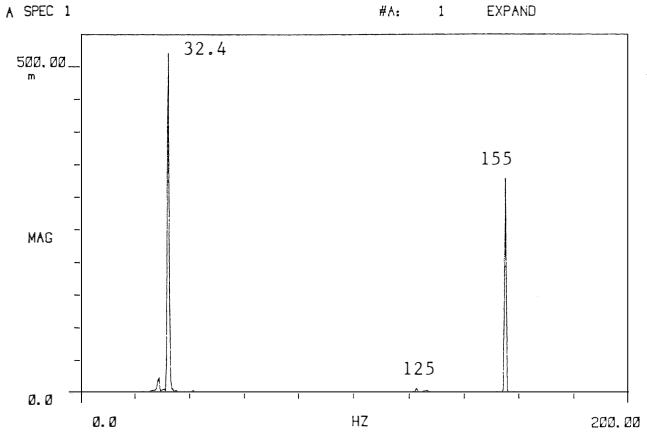

Figure 31. Steady-State Vibration Spectrum from the Lab Rotor Running at 9300 RPM.

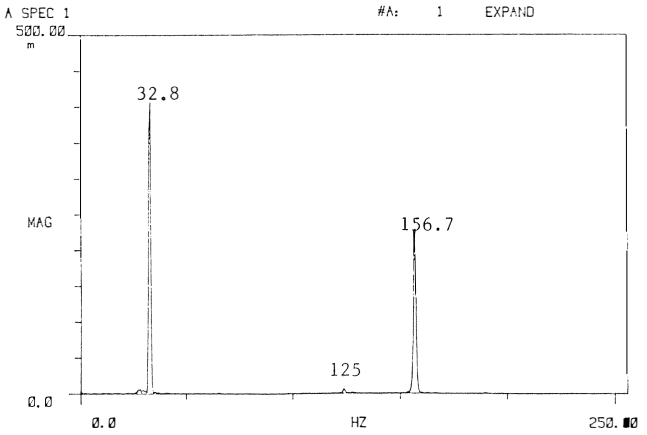

Figure 32. Transient Vibration Spectrum during Coastdown of the Lab Rotor.

decaying waveform. With the shaft speed at 9450 rpm, the shaft response to a series of hammer blows on the shaft was recorded. The recorded signal was input into an analog band-pass filter, passing all frequencies between 25 Hz and 35 Hz, and then connected into a digital oscilloscope for display. The steady state response before the hammer blows is shown in Figure 33. This waveform consists mainly of the forward whirl mode at about 30.5 Hz. The responses to two hammer blows on the shaft are presented in Figure 34. Note that the decays appear to be almost linear rather than exponential. Also note that one decay decreases faster than the other. These two responses are typical of those obtained during this test. Ignoring the inconsistencies, the logarithmic decrement would appear to be in the range of about 0.1 to 0.5.

The cause of the subsynchronous vibration is still open to question. However, it was shown before that the bearing stiffness measurements indicated that ten percent cross-coupling may be present. Including this cross-coupling in the computer model decreases the logarithmic decrement of the first mode, but not enough to make it unstable (i.e., negative). It will be shown later that the calculated values for the bearing damping used in the computer model over-estimate the damping of the bearings.

Critical Speed Comparisons

Three-Disk Rotor-Bearing System

As described earlier, this rotor-bearing test apparatus was manufactured for rotor dynamics research. The entire rotor was machined from one solid piece of steel and primarily consists of a 2.5 in diameter shaft, 52.4 in long, with three large identical disks, each 10.0 in in diameter and 5.0 in long. The bearings are a 5-shoe tilt-pad design. A photograph of the assembled test rig in place is featured in Figure 35.

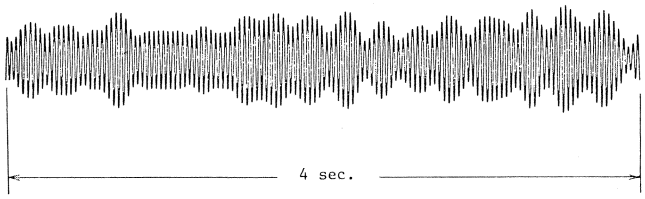

Figure 33. Time Trace of the Subsynchronous Vibration of the Lab Rotor Running at 9450 RPM.

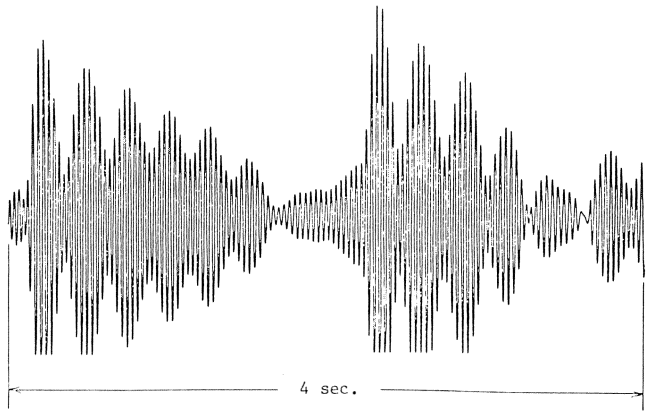

Figure 34. Time Trace from Two Hammer Blows on the Shaft of the Lab Rotor Running at 9450 RPM.

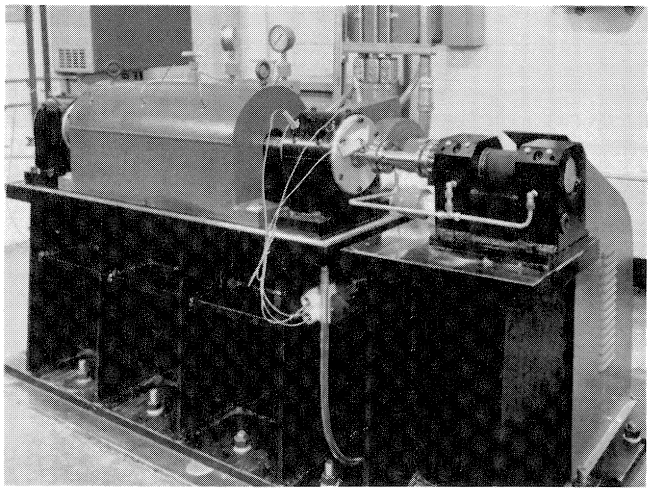

Figure 35. Assembled Test Rig, Three-Disk Lab Rotor Installed Under Cover.

Several different methods for measuring the critical speeds of this machine have been discussed. The critical speeds obtained from a coastdown of the rotor will be compared to the computed values in this analysis.

The free-free mass-elastic computer model described previously was used for the rotor shaft. Values for this model are

presented in Table 12. The measured foundation parameters are also shown in this table as well as one set of bearing parameters. All bearing stiffnesses used for this comparison were presented earlier in Table 11. Since no measurements were made for the bearing damping, calculated values for the damping were used from [10]. Before calculating critical speeds, the accuracy of a shaft model should be checked whenever possible by comparing the measured and computed free-free natural frequencies. The free-free frequencies measured and those computed are presented in Table 13.

The measured and calculated critical speeds are presented in Table 14, while the mode shapes are depicted in Figure 36. The solid curves in Figure 36 represent the calculated shaft modes and the letters "h" represent the calculated foundation displacements at each support. The measured shaft modes are shown as circles and the measured motion of the test stand is represented as a straight line. Since the third mode is vertical, the horizontal foundation has no influence and thus is not shown. The computed fourth mode at 140 Hz had no corresponding measured mode. The coastdown vibration spectrum

Table 12. Computer Shaft Model for Three-Disk Centritech Lab Rotor.

INDIVIDUAL STATION DATA

	LEN in	DO in	DI in	AWT lbf	AI in-4	AP lb-s2-in	AT lb-s2-in
1	.753	4.000	0.000	1.304	12.566	.007	.004
2	1.752	2.501	0.000	2.591	1.921	.009	.006
3	1.752	2.501	0.000	2.436	1.921	.005	.004
4	.762	4.000	0.000	2.573	12.566	.009	.006
5	1.800	2.500	0.000	2.605	1.917	.010	.006
6	2.021	2.000	0.000	2.149	.785	.004	.004
7	3.000	2.000	0.000	2.232	.785	.003	.005
8	4.998	9.900	0.000	54.773	471.531	1.728	1.160
9	2.021	2.010	0.000	55.347	.801	1.727	1.158
10	3.000	2.010	0.000	2.254	.801	.003	.005
11	4.996	9.900	0.000	54.765	471.531	1.727	1.159
12	2.012	2.005	0.000	55.316	.793	1.727	1.157
13	3.000	2.005	0.000	2.239	.793	.003	.005
14	5.004	9.900	0.000	54.845	471.531	1.730	1.162
15	2.075	2.005	0.000	55.432	.793	1.729	1.160
16	3.000	2.005	0.000	2.267	.793	.003	.005
17	2.756	2.500	0.000	3.255	1.917	.006	.009
18	1.750	2.500	0.000	3.130	1.917	.006	.007
19	1.760	2.500	0.000	2.438	1.917	.005	.004
20	2.200	2.500	0.000	2.751	1.917	.006	.005
21	1.000	1.010	0.000	1.641	.051	.003	.003
22	1.001	1.010	0.000	.229	.051	0.000	0.000
23	0.000	1.000	0.000	.111	.049	0.000	0.000

Length = 52.413 Shaft Weight = 366.683

Internal Friction Coefficient: 0

Material Properties are the Same for all Stations

Mass Density = 0.283 psi

Young's Modulus = 30.0E + 06 psi

Shear Modulus = 12.0E + 06 psi

Stations With Bearings: Number 3 and 19

BEARING DATA

KXX lb/in	KXY	KYX	KYY	CXX lb-s/in	CXY	CYX	CYY
606000	60600	−49700	497000	500	0	0	2100
606000	60600	−49700	497000	500	0	0	2100

FOUNDATION PARAMETERS

	Horizontal			Vertical		
Station	Stiffness lb/in	Damping lb-s/in	Weight lb	Stiffness	Damping	Weight
3	208000.0	55.6000	92.0	0.0	0.0000	0.0
19	208000.0	55.6000	92.0	0.0	0.0000	0.0

Table 13. Free-Free Natural Frequencies for Three-Disk Centritech Lab Rotor.

Measured	Computed (% error)
Hz	computed with program "JAZZ"
94	95 (1.1%)
207	207 (0.0%)
356	353 (−0.8%)
463	407 (−12.1%)
832	841 (1.08%)
Overall Error	Avg. = 3.02%

Table 14. Measured and Calculated Critical Speeds for the Three-Disk Centritech Lab Rotor.

Measured		Computed	
frequency Hz	log decrement	frequency Hz	log decrement
30.5	0.11	32.5 (6.56%)	0.05
108.6	0.10	103.2 (−4.97%)	0.30
125.7	0.10	128.1 (1.91%)	0.25
not measured		140.0	0.62
155.0	0.08	169.9 (9.61%)	0.40
Overall error		Avg. = 5.76%	

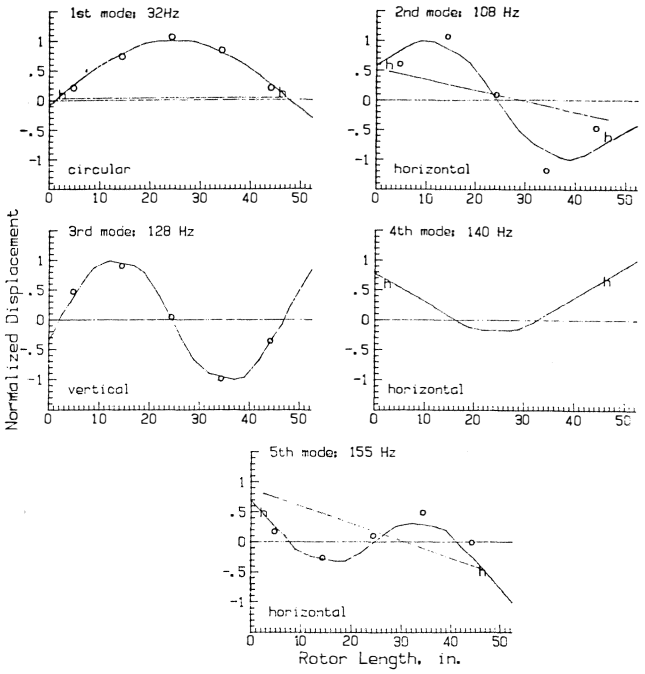

Figure 36. Comparison of Computed Mode Shapes with Mode Shapes Measured at the Critical Speeds, for the Lab Rotor.

of the test rig (Figure 21) showed no peak in the response near this frequency. The response to hammer blows on the shaft and housing (Figures 23 and 24) showed only a very slight response near a frequency of 140 Hz. This was also seen on the spectrum plots of other hammer blows recorded at other values of shaft speed. The computed logarithmic decrement for this mode is seen to be the highest of the five, and it may be that the response in this mode is being overshadowed by the two lesser damped modes immediately above and below it.

The error in the computed frequency of the 155 Hz mode was the highest error of the first four modes. This was probably due to the characteristics of the foundation. The foundation model used in the program simulated the fundamental mode of the foundation at 149 Hz. The foundation also had a second mode at 225 Hz not accounted for in the model. Since the fourth rotor mode approached this frequency, more error may be expected for this mode than for the others.

The error for the computed logarithmic decrements was rather large. The computed value was low for the first mode and high for all the others. As mentioned previously, the bearing damping coefficients were not measured and, thus, the values obtained from bearing design charts were used in all cases. The computed logarithmic decrements shown were obtained by including in the model the ten percent bearing cross-coupled stiffnesses shown in Table 11.

Another comparison was made by using the natural frequencies measured from rap tests on the shaft and bearing housing. One such set of measurements was made at a shaft speed of 4000 rpm. The measured natural frequencies and their corresponding computed values are shown in Table 15.

Table 15. Rap Tests Vs. Calculated Natural Frequencies for Three-Disk Centritech Lab Rotor at 4000 RPM.

Measured	Computed (% error)
Hz	frequency Hz
31.25	32.7 (4.64%)
110.0	105 (−4.55%)
125.0	128 (2.40%)
157.0	169 (7.64%)
Overall Error	Avg. = 4.81%

Single-Stage Steam Turbine

This is the same steam turbine rotor for which the free-free modes of vibration were described in Phase I. A photograph of the rotor showing the single large wheel located near mid-span of the shaft is presented in Figure 11. Except for the coupling hub at station 23, the computer model used for this rotor was the same, including the use of the floppy disk feature (Table 16). Since the free-free modes for the rotor with no coupling hub were measured, they can be used to check the rotor model accuracy. The agreement was excellent for the first five free-free modes as shown in Table 17.

The fluid-film bearings supporting this rotor were five-pad tilting-pad bearings with the following properties:

load on pad
L = 1.25 in
D = 3 in
arc length = 60 degrees
radial clearance = 0.0003 in
preload = 0
bearing load = 156 lb

Based on the tilt-pad bearing measurements made, a value was calculated for the vertical bearing stiffness and the horizontal stiffness was then taken as twice the vertical. The damping coefficients were also calculated using [10].

When installed, the steam turbine drives the compressor through a gear coupling arrangement. The steam turbine, therefore, has a coupling hub mounted on one end which in turn is connected to the power transmission shaft. This inertia must be carried by the steam turbine (all of the hub and part of the shaft), and, thus, must be included in the model. Detailed inertia measurements were not available, so 60 lb was used as the best estimate of the combined effect of the hub and shaft.

When this machine was purchased, the manufacturer predicted all critical speeds to be well above the top operating speed of 11,500 rpm. A rigid-support analysis performed with no coupling hub yielded a first critical speed of 13,800 rpm.

Table 16. Computer Shaft Model for Single-Stage Steam Turbine Rotor.

INDIVIDUAL STATION DATA

#	LEN in	DO in	DI in	AWT lbf	AI in-4	AP lb-s2-in	AT lb-s2-in
1	2.110	1.998	0.000	25.899	.782	.384	.194
2	2.000	1.998	0.000	1.860	.782	.002	.003
3	1.500	2.625	0.000	2.036	2.331	.004	.003
4	1.500	2.625	0.000	2.297	2.331	.005	.004
5	2.000	2.994	0.000	3.141	3.944	.008	.006
6	2.000	2.994	0.000	3.985	3.944	.012	.009
7	3.250	2.994	0.000	5.230	3.944	.015	.017
8	2.000	3.993	0.000	6.782	12.479	.028	.024
9	2.000	3.993	0.000	7.088	12.479	.037	.024
10	2.750	5.006	0.000	11.203	30.827	.080	.056
11	4.000	5.006	0.000	18.799	30.827	.152	.127
12	2.050	6.125	0.000	19.687	69.087	.194	.143
13	1.000	6.125	0.000	89.772	7269.087	10.698	5.358
14	2.050	6.125	0.000	12.716	69.087	.154	.086
15	2.700	5.006	0.000	16.067	30.827	.165	.102
16	3.000	5.006	0.000	15.875	30.827	.129	.092
17	4.050	3.990	0.000	15.521	12.441	.105	.094
18	3.100	2.995	0.000	10.256	3.950	.046	.055
19	2.300	2.995	0.000	5.383	3.950	.016	.017
20	2.300	2.995	0.000	4.586	3.950	.013	.012
21	2.550	2.500	0.000	4.064	1.917	.010	.010
22	2.000	2.500	0.000	3.160	1.917	.006	.007
23	.550	1.510	0.000	61.529	.255	.603	.303
24	.001	1.510	0.000	.140	.255	0.000	0.000
25	0.000	1.000	0.000	0.000	.049	0.000	0.000

Length = 52.761 Shaft Weight = 347.074

Internal Friction Coefficient: 0

Material Properties Are the Same for All Stations

Mass Density = 0.283 psi

Young's Modulus = 30.0E+06 psi

Shear Modulus = 12.0E+06 psi

Stations with Bearings: Number 6 and 19

BEARING DATA

KXX lb/in	KXY	KYX	KYY	CXX lb-s/in	CXY	CYX	CYY
700000	0	0	350000	1200	0	0	1500
700000	0	0	350000	1200	0	0	1500

FLOPPY DISK PARAMETERS

Station #	Stiffness (in-lb/rad)
13	240000000.0

Table 17. Free-Free Natural Frequencies for Single-Stage Steam Turbine Rotor.

Measured	Computed (% error)
Hz	Computed with "JAZZ" program
373	375 (0.54%)
602	600 (−0.3%)
1033	1055 (2.13%)
1262	1240 (−1.74%)
1998	1979 (−0.95%)
Overall Error	Avg. = 1.13%

With the coupling and tilting-pad bearing parameters included, the computed critical speeds were in closer agreement to the measured values shown in Figures 23 and 24 (Table 18). The logarithmic decrements could not be obtained from the available field data.[1]

Table 18. Measured and Calculated Eigenvalues for Single-Stage Steam Turbine.

Measured	Computed		
frequency Hz	frequency Hz	log decrement	whirl direction
140	142 (1.42%)	.18	backward
158*	150	.17	forward
180**	185	.55	backward
205	201 (1.95%)	.68	forward
Overall error	Avg. = 1.69%		

*running speed – large amplitude

**harmonic of 60 Hz electrical noise

The accuracy of the computer predicted critical speeds was excellent, in view of the fact that the coupling charcteristics were approximated and the bearing parameters were obtained in an indirect manner from laboratory measurements. Since the dynamics of the machine's foundation are unknown and were not included in the computer model, they are apparently unimportant for this particular case.

The computer whirl directions are given for this case, since the measured frequency values were taken from a spectrum generated by the turbine running at a constant 9500 rpm. Since all the measured frequencies except 158 Hz were nonsynchronous, they could represent either forward or backward whirl.

Importance of Foundation Dynamics and Bearing Asymmetry

Although foundation dynamics are apparently unimportant in the case just presented, the lab rotor was a counter example. To show the effect of the foundation, critical speeds were computed with the foundation omitted from the model. The tilt-pad bearing asymmetry was, however, retained. The resulting frequencies, compared with the values measured and the values computed with foundation dynamics included, are shown in Table 19.

Omission of the foundation impedance from the computer model eliminated two of the four predicted critical speeds in the operating range.

Many critical speed codes such as Program "CRITSPEED" described in Phase I, incorporate a symmetric model

Table 19. Critical Speeds with and without Foundation Effects for the Three-Disk Centritech Lab Rotor.

Measured	Computed	
frequency Hz	with foundation Hz	no foundation Hz
30.5	32.5	32.8
108.6	103.2	not predicted
125.7	128.1	139.8
155.0	169.9	not predicted

for bearing stiffness ($K = K_{xx} = K_{yy}$). To show the effect of this simplification, critical speeds were calculated under the assumption of symmetric bearing stiffness for both the lab rotor and the single-stage steam turbine. The symmetric bearing stiffnesses were taken to be the average of the vertical and horizontal values. In the case of the lab rotor, foundation effects were retained in the model.

The new computed values of frequency compared to the measured values and to the previously presented values computed with an asymmetric bearing model are presented in Table 20 for the lab rotor and in Table 21 for the single-stage steam turbine rotor.

For the two machines studied here, a computer model with symmeric bearing stiffness can be used with no sacrifice in critical speed accuracy when the stiffness is taken as the average of K_{xx} and K_{yy}. Additional parameter studies showed that this insensitivity of the critical speeds to bearing asymmetry is valid only when the bearings have damping values which are at least as large as those predicted using [10] for tilt-pad bearings.

Table 20. Critical Speeds with and without Bearing Asymmetry for the Three-Disk Centritech Lab Rotor.

Measured	Computed	
frequency Hz	asymmetric bearings Hz	symmetric bearings Hz
30.5	32.5	32.6
108.6	103.2	102.4
125.7	128.1	128.1
not measured	140.0	137.0
155.0	169.9	168.7

Table 21. Eigenvalues with and without Bearing Asymmetry for the Single-Stage Steam Turbine.

Measured	Computed	
frequency Hz	asymmetric bearings Hz	symmetric bearings Hz
140	142	141.7
158	150	150.6
180	185	184.8
205	201	199.6

CONCLUSION

The first two or three critical speeds for industrial machinery can be reliably predicted with errors no larger than seven

percent provided that care is taken to optimize the computer program used and to ensure that accurate values are used for the mass-elastic model, bearing properties and foundation impedance. A typical rotor-bearing system seems to be well represented by the linear mathematical model used in the transfer matrix computer program. The mass-elastic modelling guidelines set forth appear to assure accurate representation of the rotor. Reliable predictions of the critical speeds also depend on the proper choice of the bearing and foundation parameters. Dependable methods for accurately estimating these parameters are therefore required.

Asymmetric bearing stiffnesses in tilt-pad bearings can apparently be replaced by a symmetric model using the average stiffness, with little loss of accuracy for critical speed prediction, even where foundation dynamics are important. However, omission of the foundation impedance from the computer model, in cases where the foundation participates in the modes of interest, can cause some critical speeds to be missed completely.

APPENDIX

Rotor Whirl Modes and Critical Speeds

Every rotor-bearing system has a number of discrete natural frequencies of lateral vibration. Associated with each natural frequency is a mode shape, which can be thought of as a snapshot of the rotor deflection curve at the instant of maximum strain during the vibration.

When one of the natural frequencies is excited by rotor unbalance rotating at shaft speed, the shaft speed which coincides with that natural frequency is called a critical speed. In this case the rotor does not vibrate, but rather is bowed into the mode shape associated with the particular natural frequency, and whirls about its bearing centerline. To a stationary external observer, the rotor appears to vibrate, but this is simply the planar projection of the whirl orbit as seen from one side.

In mathematical terms, the natural frequencies are called eigenvalues and the mode shapes are called eigenvectors. Theoretically, a distributed mass-elastic system has an infinite number of eigenvalues and associated eigenvectors. In practice, only the lowest three or four critical speeds and associated whirl modes are excited in the operating speed range of a typical turbomachine.

The mode shapes are determined by the distribution of mass and stiffness along the rotor, as well as by the bearing support stiffnesses. The first three modes, associated with the lowest three natural frequencies of a uniform shaft, change with increasing support stiffness (Figure A-1). Note that the first two modes with low support stiffness ($K \approx 0$) involve a negligible amount of shaft bending. The same two rigid-rotor modes for a rotor with two massize disks are shown in Figure A-2. If the disks are identical and spaced equidistant from the rotor mid-span, and if the (soft) bearing supports have equal stiffnesses, then the first rigid-rotor mode will trace a cylinder and the second will trace two cones with a common apex at mid-span, as shown in Figure A-2. These cylindrical and conical modes will be somewhat modified by rotor asymmetry or by unequal bearing stiffnesses, but the terminology persists.

With a moderate amount of damping, the synchronous response plot for the rotor-bearing system of Figure A-2 would appear as shown in Figure A-3. This is a plot of the whirling amplitude measured at the bearings, caused by unbalance, as a function of shaft speed. The critical speeds are identified by the peaks of the whirl amplitude for each of the two modes.

If the shaft speed is increased beyond the conical critical, a third critical speed will be reached which involves shaft bending, as shown on the left side of Figure A-2. If the supports are very soft, this mode is essentially the same as a free-free (unsupported) mode.

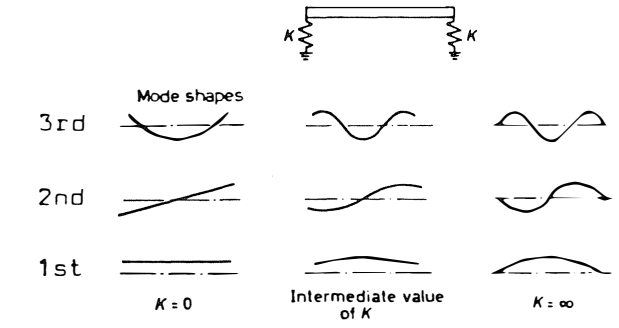

Figure A-1. Effect of Bearing Support Stiffness K on the Modes of Lateral Vibration for a Uniform Shaft.

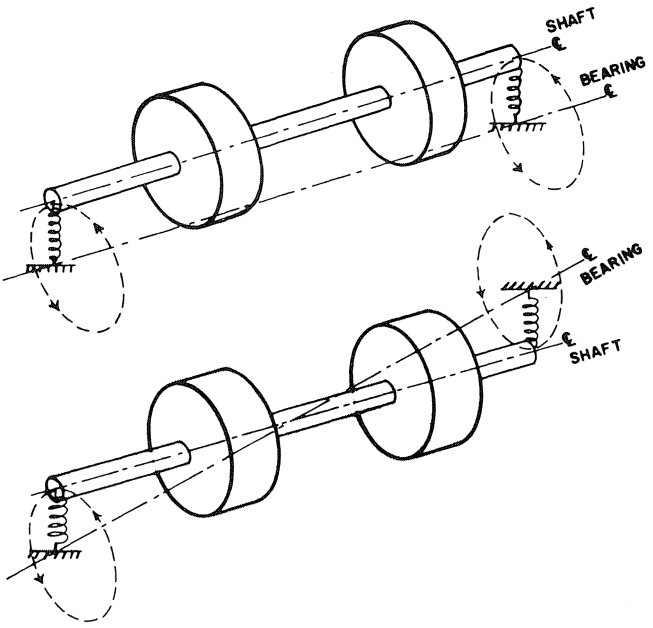

Figure A-2. Rigid-Rotor Modes of Whirling for a Symmetrical Rotor.

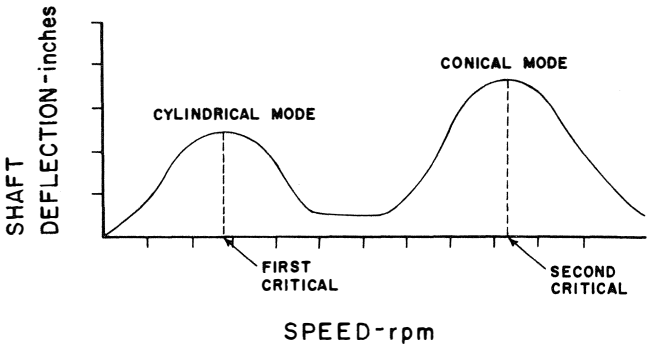

Figure A-3. Synchronous Response to Unbalance through both Rigid-Rotor Modes.

The first three critical speeds vary with support stiffness as shown in Figure A-4. This type of plot is called a critical speed map. In this case, the insensitivity of the third critical speed to support stiffness permits a range of operating speeds which does not traverse any of the critical speeds, as shown by the

vertical arrow on Figure A-4. From a rotordynamics standpoint, this is good turbomachinery design practice, but other considerations and the modern trend toward higher speeds makes it difficult to avoid approaching or traversing the third critical speed.

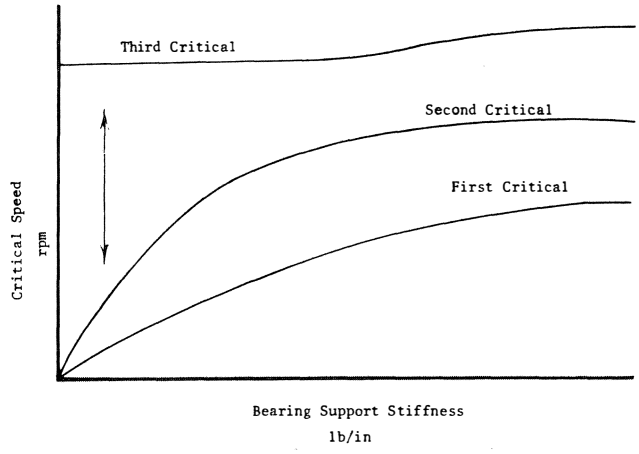

Figure A-4. Critical Speed Map for Three Modes.

For machines with oil-film bearings, there can be enough support damping to make one or both of the rigid-rotor critical speeds disappear, i.e., the peaks illustrated on Figure A-3 may not be observed. In such a case, the third calculated critical speed may in actuality become the first or second observed critical speed. This is sometimes referred to as the first bender, because of the mode shape.

If for some reason the bearing supports are stiffened, the modes become more like those shown on the right side of Figure A-1. For a symmetric rotor with two identical disks on an elastic shaft, the first two modes of operation on rigid supports are shown in Figure A-5. Mode shape (a) is approximated by a half sine wave; mode shape (b) by a full sine wave. Since rigid bearing supports cannot dissipate energy, and since internal damping in a rotor is destabilizing at high speeds, this type of design can create severe rotordynamic problems. Almost all of the flexing is in the rotor, rather than in the supports.

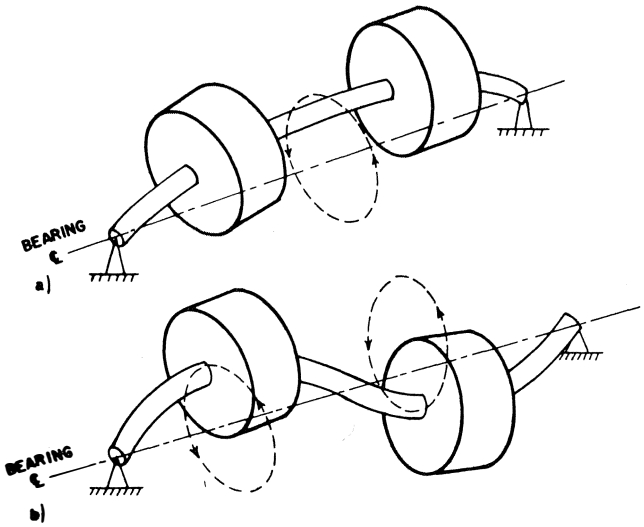

Figure A-5. First Two Rigid-Support Modes of Whirling for a Symmetric Elastic Two-Disk Rotor.

Mode shapes associated with the critical speeds of an overhung (cantilevered) disk are shown in Figure A-6. The disk is participating in the mode as a rigid body (Figure A-6a), or the disk may flex (Figure A-6b). Another possibility is that the disk may remain rigid, but its attachment to the shaft may flex. This floppy disk effect can be observed on any rotor (not necessarily overhung) which has a large wheel diameter to shaft diameter ratio.

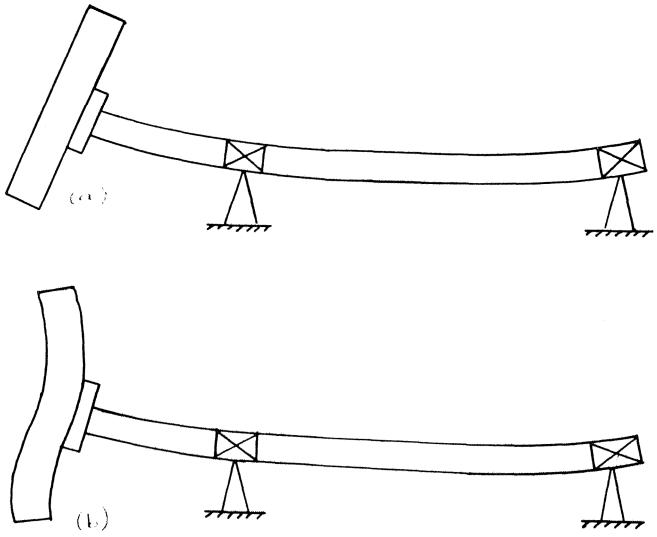

Figure A-6. Whirl Modes of an Overhung Rotor with (a) a Rigid Disk, and (b) a Flexible Disk.

REFERENCES

1. Thomas, G. B. and Littlewood, P., "A Technique for Modelling Rotors from Measured Vibration Characteristics," Proceedings of the 2nd International Conference on Vibrations in Rotating Machinery, Institution of Mechanical Engineers, Cambridge, England, pp. 445-451 (September 1980).
2. Lund, J. W., "Stability and Damped Critical Speeds of a Flexible Rotor in Fluid-Film Bearings," ASME Journal of Engineering for Industry, pp. 509-517 (May 1974).
3. Tripp, H. A., "User's Guide to Rotor 1," Technical Progress Report WRC 141-76, Shell Development, Westhollow Research Center (October 1976).
4. Dopkin, J. A. and Shoup, T. E., "Rotor Resonant Speed Reduction Caused by Flexibility of Disks," Journal of Engineering for Industry, pp. 1328-1333 (November 1974).
5. Roark, R. J., *Formulas for Stress and Strain*, 4th Edition, New York: McGraw-Hill, p. 242 (1965).
6. Wachel, J. C., "Nonsynchronous Instability of Centrifugal Compressors," ASME Paper #75-Pet-22 (1975).
7. Murphy, B. T. and Vance, J. M., "An Improved Method for Calculating Critical Speeds and Rotordynamic Stability of Turbomachinery," *Proceedings of the 10th Turbomachinery Symposium*, Texas A&M University, College Station, Texas, pp. 141-145 (1981). Also, ASME Journal of Engineering for Power, pp. 591-595 (July 1983).
8. Tripp, H. and Murphy, B. T., "Eccentricity Measurements on a 5-pad Tilting-Pad Bearing," ASLE Journal, to be published (1984).

9. Thompson, W. T., *Theory of Vibration with Applications*, 2nd Edition, Englewood Cliffs, New Jersey: Prentice-Hall, p. 76 (1981).

10. Nicholas, C. J., Gunter, E. J., Jr. and Allaire, P. E., "Stiffness and Damping Coefficients for the Five-Pad Tilting-Pad Bearings," ASLE, *22*, *2*, pp. 113-124 (April 1979).